11920–11937 *Nucleic Acids Research, 2021, Vol. 49, No. 20* *Published online 30 October 2021*
https://doi.org/10.1093/nar/gkab983

A post-transcriptional regulon controlled by TtpA, the single tristetraprolin family member expressed in *Dictyostelium discoideum*

Wenli Bai[1,†], Melissa L. Wells[2,†], Wi S. Lai[2], Stephanie N. Hicks[2], Adam B. Burkholder[3], Lalith Perera[4], Alan R. Kimmel[1,*] and Perry J. Blackshear[2,5,*]

[1]Laboratory of Cellular and Developmental Biology, National Institute of Diabetes and Digestive and Kidney Diseases, Bethesda, MD 20892, USA, [2]The Signal Transduction Laboratory, National Institute of Environmental Health Sciences, Research Triangle Park, NC 27709, USA, [3]Integrative Bioinformatics Support Group, National Institute of Environmental Health Sciences, Research Triangle Park, NC 27709, USA, [4]Genome Integrity and Structural Biology Laboratory, National Institute of Environmental Health Sciences, Research Triangle Park, NC 27709, USA and [5]The Departments of Medicine and Biochemistry, Duke University Medical Center, Durham, NC 27710, USA

Received May 06, 2021; Revised October 05, 2021; Editorial Decision October 06, 2021; Accepted October 12, 2021

ABSTRACT

Post-transcriptional processes mediated by mRNA binding proteins represent important control points in gene expression. In eukaryotes, mRNAs containing specific AU-rich motifs are regulated by binding of tristetraprolin (TTP) family tandem zinc finger proteins, which promote mRNA deadenylation and decay, partly through interaction of a conserved C-terminal CNOT1 binding (CNB) domain with CCR4–NOT protein complexes. The social ameba *Dictyostelium discoideum* shared a common ancestor with humans more than a billion years ago, and expresses only one TTP family protein, TtpA, in contrast to three members expressed in humans. Evaluation of *ttpA* null-mutants identified six transcripts that were consistently upregulated compared to WT during growth and early development. The 3′-untranslated regions (3′-UTRs) of all six 'TtpA-target' mRNAs contained multiple TTP binding motifs (UUAUUUAUU), and one 3′-UTR conferred TtpA post-transcriptional stability regulation to a heterologous mRNA that was abrogated by mutations in the core TTP-binding motifs. All six target transcripts were upregulated to similar extents in a C-terminal truncation mutant, in contrast to less severe effects of analogous mutants in mice. All six target transcripts encoded probable membrane proteins. In *Dictyostelium*, TtpA may control an 'RNA regulon', where a single RNA binding protein, TtpA, post-transcriptionally co-regulates expression of several functionally related proteins.

INTRODUCTION

Post-transcriptional regulation of gene expression is critical for the maintenance of physiological levels of mRNAs and their encoded proteins. An important component of post-transcriptional control is exerted by mRNA binding proteins, which can play diverse roles in regulation of splicing, translation, mRNA decay, mRNA localization, and other processes. A well-known group of mRNA binding proteins is the tristetraprolin (TTP) family, found throughout eukaryotes (1,2). In general, members of this family act by binding with high affinity (K_d ~1 nM) to AU-rich motifs with the optimum sequence UUAUUUAUU, typically in the 3′-UTRs of mRNA, and then promoting mRNA deadenylation and decay, and ultimately inhibition of translation. The predominant mRNA binding element in these proteins is the tandem zinc finger (TZF) domain, a 64 amino acid domain composed of two CCCH zinc fingers with highly conserved intra- and inter-finger spacings; this domain is the defining element for members of this protein family (3). Previous studies demonstrated that mutating any of the zinc coordinating residues within this TZF domain resulted in complete loss of RNA binding and loss of function in assays of deadenylation and mRNA decay (4); indeed, high level expression of such mutants often exerted an inhibitory effect on target transcript decay (4). Knocking a similar point mutation into the endogenous *Zfp36* locus (the gene encoding TTP) in mice resulted in a complete loss of function phenotype that was essentially indistinguishable from the complete knockout phenotype (5). Similar effects

*To whom correspondence should be addressed. Tel: +1 984 287 3452; Email: black009@niehs.nih.gov
Correspondence may also be addressed to Alan R. Kimmel. Email: alank@helix.nih.gov
†The authors wish it to be known that, in their opinion, the first two authors should be regarded as Joint First Authors.

of knocked-in TZF domain point mutations were found in the fission yeast *Schizosaccaromyces pombe* (6).

A second highly conserved domain found in many TTP family proteins, including those from mammals, primitive plants and protists, is a short C-terminal domain (7). This domain from human TTP was shown to interact with a central domain of the human recombinant CNOT1 protein (8). This finding provided a possible explanation for the ability of TTP and related proteins to promote deadenylation of their target transcripts, by bringing the entire CCR4–NOT complex, with its associated deadenylases, into proximity of the bound mRNA (7,8).

However, there are several pieces of evidence suggesting that this may not be the entire story of how TTP family proteins interact with CCR4–NOT complexes. For example, several studies have suggested that other domains of TTP can interact with CNOT1 (9,10), or with other members of the CCR4–NOT complex (11). Studies with the *Schizosaccharomyces pombe* Zfs1 protein, which lacks the conserved C-terminal domain, demonstrated interactions between other regions of Zfs1 and the *S. pombe* CCR4–NOT complex (12). In addition, cell transfection studies with human TTP (8) or the *Drosophila* TIS11 protein (13) suggested that loss of the conserved C-terminal domain only resulted in partial loss of mRNA decay-promoting ability. Most importantly, a knock-in mutation in mice that resulted in a C-terminal truncated TTP protein exhibited only partial loss of activity, in terms of phenotype severity, even when it was expressed in *trans* with a complete deletion allele (14). The same study showed only partial loss of activity when a recombinant C-terminal truncated version of TTP was used to activate the *S. pombe* CCR4–NOT complex (14), and when the C-terminal truncated mouse protein was used to complement the *Zfs1* null phenotype in *S. pombe* (14).

It is possible that the relatively mild phenotype seen in mice expressing only the C-terminal truncated version of TTP is due, at least in part, to the expression of three other TTP family members in the same organism. To our knowledge, the expression of multiple TTP family members is characteristic of all vertebrates, with possible functional redundancy complicating the analysis of individual protein behavior. Several model organisms express only a single TTP family member, such as *Drosophila melanogaster* (13), and yeasts such as *S. pombe* and *Candida albicans* (15–18). However, a drawback of common laboratory yeasts is that their TTP family proteins lack the typical C-terminal CNOT1 binding domain described above. It would be desirable to have an experimentally tractable, complex model organism with a single cell phase that expresses a single TTP family member, for convenient studies of protein structure and function, as well as possible 'forward genetic' studies of interacting genes.

Although *Dictyostelium discoideum* is separated from mammals by more than a billion years of evolution (19), it has a number of unique characteristics that make it an ideal model for such studies, including ease of genetic manipulation (20,21). *D. discoideum* grows as individual cells in both shaking liquid and adherent axenic cultures. However, upon nutrient depletion, *D. discoideum* initiates a developmental program leading to chemotaxis and multicell formation, cytodifferentiation, morphogenesis, and ultimately terminal differentiation into the mature fruiting body, comprised of stalk/cup cells and spores (22–25).

In this paper, we have begun to characterize the single TTP family member expressed in *D. discoideum*. This protein, which we refer to as TtpA, contains an apparently conventional RNA-binding TZF domain and a typical probable C-terminal CNOT1 binding (CNB) domain. When TtpA function was disrupted in *D. discoideum*, cells growing in culture exhibited large-fold increases in the levels of three, highly abundant transcripts, and smaller increases in the levels of three less abundant mRNAs; all six of these transcripts contained typical, often overlapping, multimeric AU-rich 'TTP family member binding sites' in their 3′-UTRs. The 3′-UTR of one of these, *sodC* mRNA, was able to confer TtpA regulation when fused with a heterologous mRNA, but mutations in the core TTP-binding motif abrogated such control. All six of these upregulated transcripts encode predicted membrane proteins, and might be described as comprising a post-transcriptional 'RNA regulon' (26–28). We used these potential target transcripts to begin to explore structure-function relationships for the TtpA protein, including the effects of a point mutation in the TZF domain, and a deletion of the C-terminal CNB domain.

MATERIALS AND METHODS

Cloning and sequencing of a full-length TtpA cDNA

Total cellular RNA was prepared from WT *D. discoideum* amebae, strain AX3, grown under axenic conditions, by seeding a liquid cell culture with 0.5 million cells/ml and harvesting them at 2 million cells/ml. Cells were pelleted, frozen, and RNA was purified using the Illustra RNAspin Kit (GE Healthcare Life Sciences) following the manufacturer's protocol. The RNA was quantitated with a Nanodrop 2000C, and 0.5 μg of total RNA was reverse transcribed using the iScript cDNA synthesis kit (Biorad), following the manufacturer's protocol. The resultant cDNA was diluted approximately 10-fold, and 1 μl was used in PCR reactions containing Platinum Taq DNA polymerase (Invitrogen) and the following primers: ttpAFwd—5′-*GATGACAGAAATTTCAAA TTCAC*-3′ and ttpARev—5′-*GTTCAAATTCAACTTG GTAAAC*-3′. These correspond to nt3894502–3894524 and 3895887–3895908, respectively, from GenBank accession number NC_007090.3 from the *D. discoideum* chromosome 4 sequence. The PCR product was subcloned using the Topo TA cloning kit (Thermo Fisher) and sequenced by Sanger Sequencing. The final sequence, which corresponded exactly to the genomic sequence in NC_007090.3, has been deposited in GenBank as accession number MT946549.

Alignment of *D. discodeum* TtpA with orthologues from other dictyostelids, social amebae and human TTP

D. discoideum is considered to be a member of the group 4 dictyostelids (19), so we aligned the predicted protein sequence of *D. discoideum* TtpA with apparent orthologues from single representatives of groups 1–3, as well as an orthologue from a more distant ameba, *Physarum*

polycephalum. GenBank accession numbers for these proteins are as follows: *P. polycephalum*, translation of genomic sequence ATCM03068633.1, bases 797–1600; *D. fasciculatum* (group 1), XP_004358709.1, with a probable missing internal segment provided by genomic read ADHC01000003.1; *D. discoideum*, MT946549 (this paper); *P. pallidum* (group 2), EFA80829.1; *Dendrocoelum lacteum* (group 3), KYR02613.1; *Homo sapiens* TTP (GenBank accession number NP_003398.3).

Solution structure modeling of the TtpA TZF domain and comparison with that of human ZFP36L2 (TIS11D)

The coordinates from the NMR structure of the RNA-bound TZF domain of ZFP36L2 (29) were appropriately mutated in constructing the initial template for TtpA, using the program Coot (30). After adding counterions, the initial model structure was solvated with 15202 water molecules. Following the protocol described previously (31), the solvated structure was equilibrated for over 20 ns with the standard Amber force field for amino acids and the PARMBSC0 force field for RNA using the program Amber.18 (32). Unconstrained molecular dynamics simulations were continued for another 100 ns at constant temperature (300K) under constant volume. The CPPTRAJ module of Amber18 (32) was used to calculate root mean square deviations. The final solution structure of the TtpA TZF domain complexed with RNA was prepared for display using the program VMD-1.9.3 (33).

Cloning, expression and purification of a recombinant TZF domain peptide from TtpA, and its use in RNA gel shift assays.

Cloning of the TZF domain from TtpA. The DNA sequence encoding the TZF domain (amino acids 225–288 in the full-length protein) of TtpA was codon-optimized for expression in bacterial cells and synthesized by Genewiz (Genewiz Genomics Laboratories). The DNA was cloned into a modified pET28/30 vector, previously described (6), encoding an N-terminal six residue histidine tag immediately followed by a maltose binding protein (MBP) tag and a TEV protease cleavage site. The final construct was verified by DNA sequencing.

Expression and purification of the TZF domain of TtpA. After transformation of the plasmid encoding the TZF domain of TtpA into *Escherichia coli* BL21 Star (DE3) cells (Invitrogen), the cells were plated onto LNT agar containing 100 μg/ml ampicillin. Bacterial cultures were grown at 37°C in LNT media in the presence of 100 μg/mL ampicillin. When the OD_{600} reached 0.6, 1 mM isopropyl β-D-1-thiogalactopyranoside (IPTG) was used to induce protein expression at 22°C for 16 h. Cells were centrifuged at 3600 rpm at 4°C for 15 min and pellets were stored at –20°C. Frozen cell pellets were resuspended in 50 ml of buffer containing 20 mM sodium phosphate, pH 8.0, 100 mM potassium chloride, 10 mM imidazole, 5% glycerol, and one EDTA-free protease inhibitor tablet (Roche) and lysed by sonication for 30 s intervals, for a total of four intervals, on ice. Following centrifugation at 35 000 rpm at 4°C for 30 min, supernatants were applied to a 5 ml HisTrap HP column (Cytiva Life Sciences), washed with 5 column volumes of buffer and eluted in the same buffer containing 400 mM imidazole. After incubation with tobacco etch viral (TEV) protease overnight at 4°C in the presence of 3 mM dithiothreitol, proteins were diluted into buffer A containing 20 mM sodium phosphate, pH 7.6, 30 mM potassium chloride, 25 μM zinc sulfate, 2 mM 2-mercaptoethanol, and 5% glycerol. Subsequently, protein was loaded onto a HiTrap Heparin HP column (Cytiva Life Sciences) and eluted in a linear gradient from 0% to 80% buffer NT (buffer A + 1 M potassium chloride). After concentration utilizing a 3000 MWCO Vivaspin 20 centrifugal filtering device (Cytiva Life Sciences), protein was applied to a Superdex 200 10/300 GL size-exclusion column (Cytiva Life Sciences) equilibrated in 20 mM sodium phosphate, pH 7.6, 100 mM potassium chloride, 25 μM zinc sulfate, 2 mM 2-mercaptoethanol and 5% glycerol. Fractions containing purified TZF domain were pooled and concentrated using a 3000 MWCO Vivaspin 20 centrifugal filtering device (Cytiva Life Sciences). Purified protein was buffer exchanged into 20 mM sodium phosphate, pH 7.6, 100 mM potassium chloride, 25 μM zinc sulfate, 2 mM 2-mercaptoethanol and 5% glycerol. Concentrated proteins were stored at –80°C after flash freezing in liquid nitrogen.

RNA electrophoretic mobility shift assay (EMSA). RNA electrophoretic mobility shift assays were carried out as described previously (34). Briefly, the purified TZF domain (1 and 0.5 μg) of TtpA was incubated with 0.6 ng of single stranded 5′-biotin-labeled probe (Horizon Discovery) based on the 3′-UTR of mouse tumor necrosis factor alpha (TNF) mRNA (bp 1309–1332 from GenBank accession number X02611). All assays were carried out using either a multisite RNA probe with the sequence 5′-biotin-UUAUUUAUUUAUUAUUUAUUUAUU-3′, or a single site probe, 5′-biotin-UUAUUUAUU-3′, as indicated. Reactions were incubated for 20 min at room temperature, and then run on a 5% nondenaturing Criterion TBE polyacrylamide gel (Bio-Rad) for 1 h at 150 V at 4°C. After transfer to a Biodyne B nylon membrane (Thermo Fisher Scientific), ARE probe and protein-ARE complexes were detected using a streptavidin-HRP conjugated antibody within the Chemiluminescent Nucleic Acid Detection Module (Thermo Fisher Scientific), according to the manufacturer's protocol, after exposing to film.

Cloning of mammalian expression vectors for an amino-terminal truncated version of TtpA and its mutants, and transfection into HEK 293 cells

DNA fragments of *H. sapiens*-biased codons encoding the WT TtpA protein, the TZF domain mutant C246T, and the CNOT1 binding domain mutant (RTANTKTTC at the TtpA C-terminus, in which the underlined polar residues indicate substitutions for the hydrophobic amino acids L, I, F and I, respectively), were synthesized by Genewiz (Genewiz Genomics Laboratories). These DNA fragments, including an initiator methionine at M103 in the WT TtpA sequence), were inserted between sequences encoding GFP and the bovine growth hormone 3′-UTR at the Asp718 and

XhoI sites in vector CMV.EGFP.BGH3′. The last residue of GFP was followed by the Asp718 site, which was followed by TtpA M103 in frame.

Co-transfection assays were performed (35) using human HEK 293 cells to assess the ability of these TtpA expression constructs (5 ng DNA per 100 mm dish) to influence the stability of a reporter mRNA, expressed by Mlp-TNF3′ (3 μg DNA together with 2 μg of vector DNA BS + per dish) as described (14). Expression and subcellular localization of these GFP-TtpA fusion proteins, and GFP alone, were visualized using an EVOS fluorescence inverted microscope (Advanced Microscopy Group) 48 h after the transfection. At about the same time the cells were treated without or with actinomycin D (Sigma, ActD, 5 μg/ml) for 1 h. After rinsing in ice-cold PBS, the cells were lysed in lysis buffer (Illustra RNAspin mini, GE Healthcare). The lysates from cells transfected with the same constructs and the same treatment (3 dishes) were pooled, and cellular RNA was extracted according to the manufacturer′s protocol.

Northern blotting with a *Marcksl1* cDNA probe (36) was visualized by autoradiography and quantitated using a PhosphoImager and mRNA-probe bound volume (ImageQuant, Molecular Dynamics). The probe-bound volume of the *Marcksl1-Tnf3′* fusion mRNA was first normalized by the bound volume of endogenous *Marcksl1* mRNA, and the results were presented as either steady state levels, or levels after 1 h of treatment with ActD, as described (13,14).

Mutagenesis of *ttpA*

WT cells (Ax3) were used to generate four different putative null mutations in the endogenous *ttpA* gene, as well as a 'reversion of null' mutant and a C-terminal truncation mutant. For predicted null mutations within the TZF domain, the 20 nt sequence 5′-GAGACTGGTGTTTGT AGATA-3′ was cloned into the CRISPR vector pTM1285 (37). To create $ttpA^{C240ins}$, a mutant in which an insertion containing the blasticidin resistance sequence was inserted into the TZF domain, this plasmid (pTM1285-Ttp A) and a plasmid comprised of TtpA sequences including 674 nt upstream of the proposed CRISPR site, and 518 nt of downstream sequence (3894503–3895176 and 3895391–3895908, respectively, from GenBank accession number NC_007090.3), surrounding a basticidin S deaminase sequence from the CRISPR vector (37), were co-transfected into WT cells. Individual clones resistant to blasticidin (10 μM) were selected and sequenced. Two additional putative null strains, $ttpA^{E236fsx}$ and $ttpA^{Y242fsx}$, were made by creating frame shift mutations near the beginning of the TZF domain. These strains were created by transfecting WT cells with pTM1285-TtpA, and identifying and sequencing frame shift mutants. One strain selected for further use, $ttpA^{E236fsx}$, was missing two bases at the site of E236 in the TtpA protein sequence, but retained a protospacer adjacent motif (TGG). To restore this presumed null strain back to WT, we cloned this mutant target sequence into pTM1285, and co-transfected the cells with a 200 nt single-stranded DNA oligonucleotide from the *ttpA* sequence, representing nt 3895125–3895322 from GenBank accession number NC_007090.3. The resultant strain, $ttp^{E236fsx\text{-}rev}$, was confirmed to consist of the WT sequence. To create a fourth presumed null mutant, we mutated one of the key cysteine residues within the TZF domain to serine ($ttpA^{C231S}$). In this case, WT cells were co-transfected with the CRISPR plasmid pTM1285-TtpA, along with a 200 nt single-stranded DNA oligonucleotide from *ttpA* that contained the mutant sequence 5′-ACTGA ATTGTcTAGgTCTTTT-3′. Sequencing of one of the resulting clones confirmed that cysteine 231 within the TZF domain was changed to serine.

To create the C-terminal truncation strain $ttpA^{D450trx}$, the target sequence from near the 3′-end of the *ttpA* open reading frame, CAATTTGTTCAAATTCAACT, was cloned into pTM1285. This was transfected into WT cells with a 200 nt single-stranded DNA oligonucleotide that also encoded a myc epitope tag: 5′-TTCTTGGTCAA GTGATGAGGCCTCATCAACTGCACCAAACTCT TCTTTTAATCAATTAAAATCTTCTGCTCCTCCAA TTTTAAAGAAAGAAGATaTCTCTGAACAAAAA CTCATCTCAGAAGAGGATCTGTGGTAAACAAA AATAAAAATAAAAAAATAAAAAATAAAAAATA AAAAAACAAAAAAAAAAAAAAAAAAAA-3′. The correct placement of the C-terminal deletion, and the presence of the epitope tag sequence, were confirmed by genomic DNA sequencing.

RNA-Seq experiments

Total RNA was isolated from the indicated cultures using the Illustra RNAspin Kit (GE Healthcare Life Sciences) following the manufacturer's protocol. Total RNA was quantitated with a Qubit fluorometer, and 250 ng of each sample was transcribed to generate cDNA libraries using the Illumina TruSeq RNA Kit (Illumina Inc, San Diego, CA) following the manufacturer's Low Sample (LS) protocol with the following modifications: 2 min of centrifugation were used during the bead drying steps and 12 cycles were used to enrich DNA fragments. The resulting libraries were sequenced following the manufacturer's protocol using the NextSeq 500 High Output Kit (150 cycles) on the Illumina NextSeq 500 System or using the NovaSeq 6000 SP Reagent Kit (200 cycles) on the Illumina NovaSeq 6000 System (Illumina Inc., San Diego, CA). Alternatively, total RNA was quantitated with a Qubit fluorometer, and 1 μg of each sample was transcribed to generate cDNA libraries using the TruSeq Stranded mRNA Sample Prep Kit (Illumina Inc, San Diego, CA) following the manufacturer's protocol with the following modifications: 10 cycles were used to enrich DNA fragments to minimize the risk of over-amplification, and dual-indexed barcode adapters were applied to each library. Libraries were pooled in an equimolar ratio for sequencing on the Illumina HiSeq 4000 System (Illumina Inc., San Diego, CA).

Reads were filtered to remove pairs in which either mate's mean base quality fell below 20, and were aligned to the *D. discoideum* reference assembly downloaded from dictyBase.org in January, 2018. Alignments were performed as data became available using either STAR 2.5.2b or 2.6.0c. Other than the following, default parameters were utilized in all cases: –outMultimapperOrder Random, –outSAMattrIHstart 0, –outFilterType BySJout, –outSAMstrandField intronMotif, –outFilterIntronMotifs

RemoveNoncanonical. Per-gene fragment counts were determined in a strand-independent manner using featureCounts 1.5.1, excluding chimeric pairs and reads with mapping quality less than 10 (-Q 10, -C, -p, -s 0). Gene annotations utilized for this purpose were downloaded from dictybase.org in March, 2018. Read counts were normalized using DESeq2 1.18.1, running under R 3.4.0. Differential expression analyses were performed using DESeq2′s standard workflow with default parameters (DESeqDataSetFromMatrix, estimateSizeFactors, estimateDispersions, nbinomWaldTest, results).

NanoString experiments

The NanoString nCounter technique allows for mRNA quantitation without amplification over a large dynamic range (38,39). For purposes of these and future experiments, we constructed a custom codeset using the mRNA sequences for the putative TtpA targets *sodC*, *DD3-3*, and *DDB_G0281067*, for GFP, and for *ttpA* mRNA itself. An important component of these analyses is the use of a collection of housekeeping transcripts for internal normalization. For this purpose, we analyzed all of the samples from the surface growth RNA-Seq experiments comparing null mutants and WT cells, and chose transcripts whose average abundances were in a range around that of *sodC* mRNA in WT cells from the RNA-Seq data; whose average levels differed less than 4% between null mutant and WT; and whose variability among individual samples was very low. We ultimately chose 14 transcripts for this analysis, including the following genes: *DDB_G0275459*, *DDB_G0276821*, *cmfB*, *copG*, *dscE*, *nhp2l1, sdhD, snpA, tom70, trxC, ubqA, vatA, vatB,* and *vatE*. Cells from the indicated experimental conditions were frozen and used for RNA purification as described above, and then analyzed by NanoString Technologies, Seattle, WA. The copy number calculation for *ttpA* mRNA from WT cells under surface growth conditions in normal medium was based on the assumptions found in https://www.nanostring.com/wp-content/uploads/2020/12/Gene_Expression_Data_Analysis_Guidelines.pdf, using the estimated RNA amounts per cell in *Dictyostelium* from (40).

3′-UTR analyses

For the three most highly up-regulated transcripts, *sodC*, *DD3-3* and *DDB_G0281067* mRNAs, we predicted 3′-UTR sequences based on a combination of genomic sequences, ESTs, SRA reads and UCSC browser tracks from the RNA-Seq data. We then searched the available dictyostelids in GenBank for proteins encoded by orthologues of the three 'top tier' targets listed above, and identified predicted 3′-UTRs for each of these transcripts from the species depicted on the tree, based on 243 nt of genomic 3′ sequences following the stop codon. Each 3′-UTR was searched for potential TTP family member binding sites, with the minimal sequence of UAUUUAU. Similar techniques were used to predict 3′UTRs for the 'second tier' *cybA*, *noxA* and *DDB_G0278313* mRNAs.

Generation and analysis of cells expressing GFP-sodC 3′-UTR fusion plasmids

The plasmid vector and WT cells were obtained from the Dicty Stock Center, Northwestern University, Chicago, IL, USA, and the NBRP Resource Center, Nenkin, Japan. Approximately 950 nt of the genomic region containing the *sodC* mRNA 3′-UTR (estimated as 117 b) was amplified from WT cell genomic DNA, and cloned into the pTX-GFP vector at the C-terminal end, resulting in plasmid pTX-GFP-3'-sodC-UTR-Wt. This plasmid was mutated using PCR mutagenesis, changing the original 3'-UTR TtpA binding site region from TTATTTATTTAT TTATTTATTT to TTtTTTtTTTATTTtTTTATTT. Both plasmids were used to transfect WT and *ttpA* mutant cells under selection of G418. GFP expression was confirmed by fluorescence microscopy and western blotting with anti-GFP antibodies (abcam, catalog number E385), with an antibody directed at β-actin (Santa Cruz Biotechnology, catalogue number Sc-47778) serving as an internal control.

Northern blotting of TtpA target transcripts from WT and mutant cells

Total RNA was isolated from the WT and mutant cells ($ttpA^{E236fsx}$) in surface culture using the Illustra RNAspin Kit (GE Healthcare Life Sciences), following the manufacturer's protocol. Each gel lane was loaded with 5 μg of total RNA for northern blotting. As a negative control, 5 μg of HEK 293 cell total RNA was also loaded to an adjacent lane. DNA fragments of native sequence encoding portions of the DD3-3 protein (985 bp), the entire DDB_G0281067 protein (904 bp), the entire SodC protein (1225 bp), or the entire UbaA protein (1146 bp) were synthesized by Genewiz as templates to make alpha-[^{32}P]-labeled probes for northern hybridization. We also repeated the northern blots after cleaving each of these three transcripts near the 3′-ends, with sequence-specific primers and RNAse H, and probed these with labeled 3′-specific probes as described (14). For DD3-3, the following numbering positions were based on the genomic sequence starting from the initiator ATG, from GenBank accession number NC_007090.3:c212062. From that point, the locations of the complimentary oligonucleotides of 16–17 nt each were at positions 1390, 1454, 1521, and 1672. The northern probe was approximately 298 nt starting at position 1760. For SodC, the following positions were based on the same organization, from GenBank accession number NC_007090.3:c111541. From that starting point, the locations of the complimentary oligonucleotides of 17–19 nt each were at positions 933, 1058 and 1119 of this sequence. The northern probe was based on nt 1136 to 1458 of this sequence. For DDB_G0281067, the following positions were based on the same organization, from GenBank accession number NC_007089.4:c4003396. From that starting point, the oligonucleotides of 15–17 nt were complementary to sequences starting at positions 690,762, 783 and 834. The cDNA probe was designed to hybridize to nt 852–1123 of this sequence. Double-stranded DNA templates for making labeled probes were synthesized by Genewiz, Inc., and DNA oligonucleotides complimentary to the target mRNA

sequencies were synthesized by Invitrogen Life Technologies.

Western blotting of DD3-3 in *ttpA* WT and mutant cells

Whole cell extracts were prepared by lysing cells in a buffer consisting of 20 mM Tris–HCl (pH 7.2), 1% SDS, 1 mM EDTA and 1 protease inhibitor cocktail tablet/25 ml buffer (Roche). Protein concentrations were determined by using a Nanodrop 2000C. Total protein (2 μg) was mixed with 1/5 volume of 5 X SDS sample buffer (0.25 M Tris–HCl (pH 6.8), 10% SDS, 50% glycerol, 0.25% bromophenol blue, and 5% 2-mercaptoethanol) and boiled for 5 min. Lysates were separated on Any kD Criterion Tris-HCl precast gels (Bio-Rad Laboratories) and transferred onto nitrocellulose membranes. Membranes were blocked in 5% milk in TBST (Tris-buffered saline with 0.1% Tween-20) and incubated at 4°C overnight with two different rabbit antisera (1:2000 dilution) raised against a synthetic peptide from *D. discoideum* DD3-3 (GenBank accession number BAD93186.1, amino acids 404–419, conjugated with KLH (Covance)), or their respective pre-immune sera. This was followed by incubation at room temperature with goat-anti rabbit-HRP antibody for 1 h (Biorad) (1:20 000). Proteins were visualized with Advansta WesternBright ECL substrate (Advansta).

Membrane topology predictions

Predicted protein sequences for the six target transcripts described in this paper were entered into the program Phobius (http://phobius.sbc.su.se/), and the default parameters were used to calculate the predicted membrane topology for each of the proteins.

RESULTS

D. discoideum TtpA

We previously identified a single predicted protein of the TTP family in *D. discoideum* (7). Here, we functionally characterize the *D. discoideum* protein and, in accord with the TTP family designation and common *D. discoideum* nomenclature, we term this protein TtpA, and the gene as *ttpA* (annotated as DDB_G0285973 (20,21)). This protein contains a typical TZF domain with correct internal spacing and conserved residues, and a predicted C-terminal CNOT1 binding (CNB) domain (Figure 1A) (7). We confirmed the absence of introns in this gene by cloning and sequencing a cDNA from *D. discoideum* cells (GenBank accession number MT946549). Based on the RNA-Seq data described below and these sequences, the full-length mRNA for this gene corresponds to GenBank accession numbers NC_007090.3:3893864–3896145.

The dictyostelids can be placed into four evolutionary groups based on sequence relationships to amebozoa outgroups (19,41). Group 4 is thought to have evolved most recently, with *D. discoideum* its best-studied member (19). We compared the TtpA sequence to representative proteins from groups 1–3 (Figure 1A). There was strong conservation within the 64 amino acid TZF domain (red box in Figure 1A), and a similarly conserved C-terminal putative CNB domain (green box in Figure 1A). Another region of conservation was the pink shaded region in Figure 1A, reminiscent of the tryptophan clusters in TTP that may interact with CNOT9 (11). The shortest family member found to date among social amebae is from the acellular ameba *Physarum polycephalum* (42) (GenBank accession number ATCM03068633.1, bases 797–1600), with a predicted protein of 268 amino acids (Figure 1A).

Alignment of TtpA with human TTP (GenBank accession number NP_003398.3) shows a high level of sequence conservation in the TZF and CNB domains (Figure 1B), with the latter domains being located at the extreme C-termini of the proteins from both species.

Figure 1B also illustrates the locations of the mutations we made in the endogenous *ttpA* locus, using CRISPR-Cas9 technology, including: A loss of function mutation caused by the insertion of a blasticidin-resistance element after the second cysteine in the TZF domain ($ttpA^{C240ins}$); a point mutant changing cysteine 231, a critical coordinating residue for zinc ions, to serine ($ttpA^{C231S}$); a loss of function frame shift mutation within the TZF domain, at E236 ($ttpA^{E236fsx}$); a reversion mutation that converted this frame shift back to the normal open reading frame ($ttpA^{E236fsx\text{-}rev}$); and another loss of function frame shift mutation within the TZF domain, at Y242 ($ttpA^{Y242fsx}$). We also made a C-terminal truncation mutant, in which the putative CNB domain was removed, leaving an otherwise intact protein ($ttpA^{D450trx}$).

RNA binding and solution structure modeling

We expressed a recombinant TtpA TZF domain peptide in fusion with maltose binding protein in *E. coli*, and purified it through His-tag affinity binding, proteolytic cleavage of the fusion partner, and gel filtration (Figure 2A). As shown by electrophoretic mobility shift assays, and similar to human TTP, the recombinant peptide bound to a biotin-labeled RNA probe corresponding to the core binding domain of the known TTP target transcript, *Tnf* (5′-biotin-UUAUUUAUUUAUUAUUUAUUUAUU-3′) (Figure 2B). The TtpA peptide also bound to a biotinylated RNA probe containing a single TTP family binding site (5′-biotin-UUAUUUAUU-3′) (Figure 2C). Using fluorescence anisotropy, we estimated a K_d for this single site interaction of ∼1.8 nM at 24°C (data not shown), similar to those found using TZF domain peptides from other species (13,17,18). Solution structure modeling of the TtpA TZF domain, in complex with the optimal single TTP binding sequence of UUAUUUAUU, was based on the original structure of the human TIS11D (ZFP36L2) TZF domain in complex with the same oligonucleotide (29). The predicted structure of the *D. discoideum* TZF domain in complex with RNA (Figure 2D) was very similar to the structure of the human ZFP36L2 TZF domain complexed to the same oligonucleotide (Figure 2E), with a root mean squared deviation of 2.1 Å for the backbone atoms. Taken together, these data suggest that the *D. discoideum* TtpA TZF domain behaves like those of other eukaryotes that have been studied to date in terms of high-affinity binding to the preferred binding sequence in single-stranded, unstructured RNA.

We previously performed similar solution structure modeling of the predicted TtpA C-terminal CNB domain and its

Figure 1. Sequence and domain structure of TtpA from *D. discoideum.* (**A**) shows the complete predicted amino acid sequences of TtpA from *D. discoideum*, a representative of the group 4 dictyostelids, and representatives of groups 1–3; group numbers for each are shown in parentheses after each species name. These are compared with a more distantly related acellular social ameba, *P. polycephalum*, chosen because it has the shortest TtpA protein length we have identified to date among the social amebae. The alignments used the ClustalW conventions of asterisks for amino acid identity; colons for chemical similarity; and single dots for less chemical similarity. The conserved 64 amino acid TZF domains are outlined in red, and the conserved C-terminal CNOT1 binding (CNB) domains are boxed in green. Another moderately conserved domain of unknown function is highlighted in pink. GenBank accession numbers for these proteins are as follows: *P. polycephalum*, translation of genomic sequence ATCM03068633.1, bases 797–1600; *D. fasciculatum*, XP_004358709.1, with a probable missing internal segment provided by genomic read ADHC01000003.1; *D. discoideum*, MT946549 (this paper); *P. pallidum*, EFA80829.1; *D. lacteum*, KYR02613.1. (**B**) shows alignments of the TZF (red brackets) and CNB domains (green brackets) from *D. discoideum* TtpA and *H. sapiens* TTP (GenBank accession number NP_003398.3), with the zinc coordinating cysteines and histidines highlighted in red. The locations of the six *ttpA* mutants described in this paper are indicated by the red arrows, with abbreviations as follows: C231S, replacement of cysteine 231 with serine in GenBank accession number MT946549; E236fsx, a frame shift mutation after glutamate 236; E236fsx-rev, a correction of that frame shift mutation and reversion to the normal sequence; C240ins, insertion of a foreign sequence after cysteine 240; Y242fsx, a frame shift mutation after tyrosine 242; and D450trx, a truncation of the protein after aspartate 450. See the text for further details.

predicted interaction with a central 'hydrophobic pocket' of *D. discoideum* CNOT1 (7). This resembled the crystal structure of the human TTP C-terminal peptide interacting with three central helices of the human CNOT1 protein (8).

Protein expression and activity in human HEK 293 cells

When expressed in human HEK 293 cells, full-length TtpA with an N-terminal GFP fusion was cleaved at a site quite close to the C-terminus of the GFP. We therefore made new expression constructs, in which the methionine at position 103 in the WT TtpA protein was fused downstream of GFP. We also made two mutant versions of this fusion, including a C246T mutation in the TZF domain that should disrupt RNA-binding, and a C-terminal mutation (mut CNBD) that should prevent binding to the hydrophobic pocket of the CNOT1 protein (7). In this case, the *D. discoideum* WT C-terminal sequence, R**L**A**I**FK**T**ICSNSTW, was replaced by R**T**A**N**TK**T**TCSNSTW, with the four key hydrophobic amino acids in bold type replaced as indicated.

GFP alone was expressed in both nuclear and cytosolic compartments of HEK 293 cells (Figure 3A, GFP), whereas the WT and mutant GFP-TtpA fusion proteins were localized predominantly in the cytosol (Figure 3A, WT, C246T and mut CNBD). In a separate experiment, the WT protein was localized to the nucleus after treatment of the cells with leptomycin B, an inhibitor of CRM1-dependent nuclear export (43) (data not shown). It thus appears that, like many members of this protein family, TtpA contains a nuclear export sequence that promotes cytosolic localization (44). All three constructs expressed relatively similar levels of the fusion proteins, as determined by western blotting, although the TZF domain point mutant was expressed at slightly lower levels; there was also evidence of proteolytic fragments in all cases (Figure 3B).

We then tested the ability of the WT and mutant TtpA proteins to promote mRNA decay in mammalian cells, using as a 'target' a fusion mRNA based on the protein coding region of the mouse MARCKS-like 1 (*Marcksl1*) gene fused with a mouse *Tnf* mRNA 3′-UTR that contains multiple potential TTP binding sites (14). Northern blotting allows for the normalization of expression based on endogenous *Marcksl1* mRNA, which migrates at a slightly larger size in this gel system. GFP was used as a negative control. The *Marcksl1* promoter is susceptible to actinomycin D (ActD) inhibition, allowing mRNA decay assessment in addition

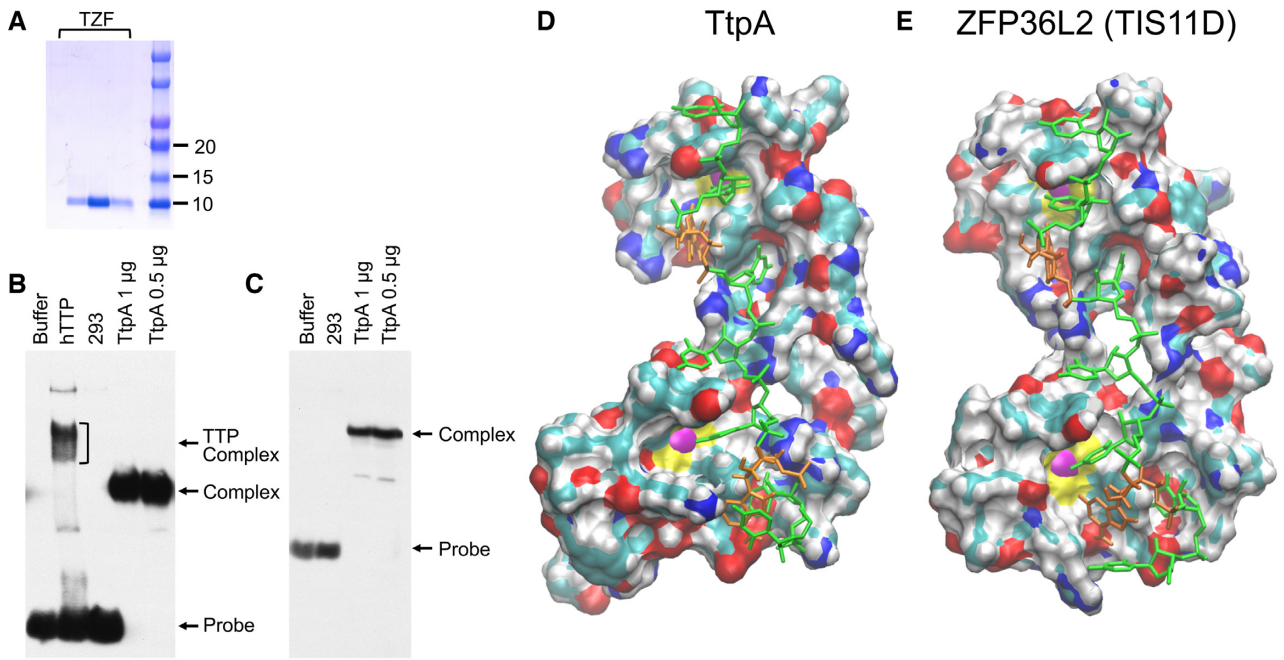

Figure 2. RNA binding of a recombinant TtpA TZF domain and its solution structure model complexed to RNA. (**A**) shows the purified TtpA TZF domain peptide after gel filtration, with the Coomassie blue stained gel showing five consecutive fractions off the column. Molecular size markers to the right represent M_r X 1000. (**B**) shows an RNA gel shift experiment using a biotinylated single-stranded RNA probe derived from mouse *Tnf* mRNA that contains two potential TTP family member binding sites (67). The first lane (Buffer) represents the probe alone (Probe) incubated in buffer. The second lane (hTTP) contains 3 µg of a human HEK 293 cell cytosolic extract from cells expressing full-length human TTP. The TTP-probe complex is labeled; multiple bands are thought to reflect multisite TTP phosphorylation. The third lane (293) contains an equivalent amount of a human HEK 293 cell cytosolic extract alone. The fourth and fifth lanes contain the purified TtpA TZF domain peptide at 1 and 0.5 µg, respectively. The free probe and the TZF domain peptide—probe complex are indicated. (**C**) shows a similar gel shift experiment with a single binding site biotinylated probe, 5′biotin-UUAUUUAUU-3′. Note the complete shift of probe into the gel in the lanes containing the TtpA TZF domain peptide in both B and C. (**D**) shows a solution structure model of the 64 amino acid TZF domain from TtpA, in complex with the presumed optimal RNA sequence UUAUUUAUU, and (**E**) is the analogous structure from the human ZFP36L2 (TIS11D) protein as described in (29). The single-stranded RNA chain is in light green, with the 3′-end at the top, except that the two A residues are in orange. Color code for atoms in proteins: Red – oxygen; blue – nitrogen; cyan – carbon; gray (or off-white)—hydrogen. Generally, oxygens are slightly negatively charged, and most of the nitrogens shown are from lysines or arginines and they are slightly positively charged. Yellow represents the sulfur in methionine and cysteine. The two zinc ions in each structure are shown in purple.

to steady state analyses. In a single illustrative experiment (Figure 3C) and in average data taken from three identical experiments (Figure 3D), the WT GFP-TtpA protein caused decreases in steady state levels of the target transcript by more than 30% compared to GFP alone (compare lanes 1 and 3 of Figure 3C; see also Figure 3D). Further, after 1 h of ActD treatment to suppress new transcription, GFP alone caused average decreases of target transcript mRNA of only a few percent, whereas the WT TtpA fusion protein caused a significant decrease of more than 50% relative to the GFP control ($P = 0.002$; compare lanes 2 and 4 of Figure 3C; see also Figure 3D). The TZF domain point mutant caused little change in either steady state target transcript levels, or levels after 1 h of Act D treatment, compared to GFP alone (Figure 3C, compare lanes 5 and 6 to lanes 1 and 2; see also Figure 3D). These findings parallel those seen with mammalian and insect TTP family proteins, indicating that the *Dictyostelium* TtpA protein exhibited typical TTP-like activity in this human cell expression system, with the TZF domain point mutant being inactive.

Although highly conserved across evolution (7,8), the precise function of the C-terminal CNB domain has been less clear. C-terminal CNB domain mutants in mammalian TTP and *Drosophila* Tis11 showed substantial residual activity in this assay system compared to TZF domain point mutants (8,13,14). In contrast, the C-terminal CNB domain mutant of TtpA showed minimal effects on steady state target transcript levels, and although levels after 1 h of Act D treatment were slightly decreased compared to GFP alone, these differences were limited compared with WT TtpA (Figure 3C, lanes 7 and 8, and Figure 3D). The data suggest a more significant contribution of the C-terminal CNB domain to TtpA activity in this species than in mammals or flies. Nonetheless, despite apparent sequence conservation between only the TZF and CNB domains of the *Dictyostelium* and mammalian proteins, TtpA is able to confer TTP-like stability regulation when ectopically expressed in mammalian cells.

Loss-of-function mutants in *D. discoideum* TtpA

When the various *Dictyostelium* null mutants were grown in shaking liquid culture, we observed decreased cell proliferation at several temperatures, and enlarged nuclei with increased numbers of DAPI-staining nuclear foci (Supplemental Figure S1). These phenotypes were also seen with the TZF domain point mutant $ttpA^{C231S}$. The same changes were prominent in the frame shift null mutant $ttpA^{E236fsx}$,

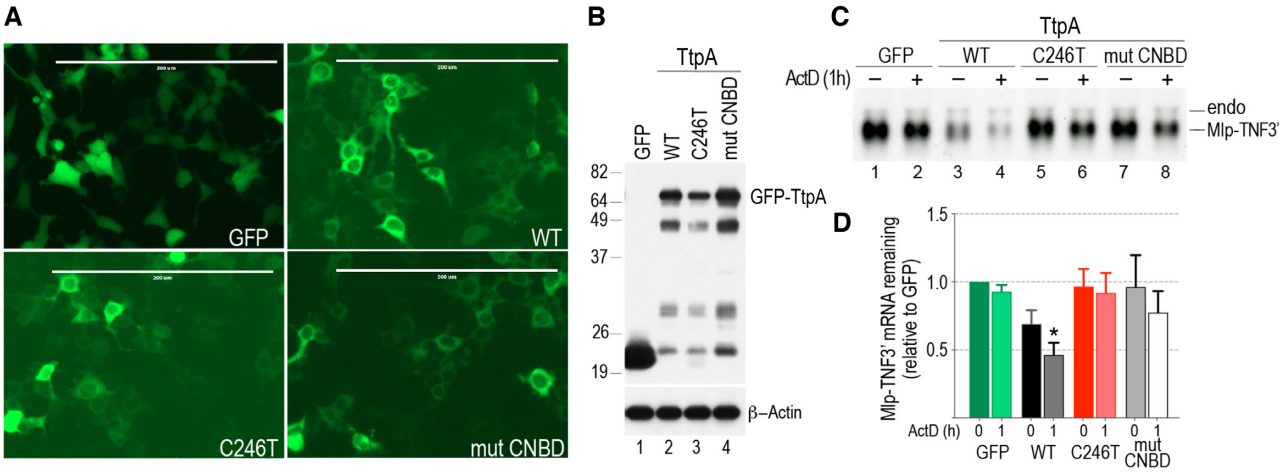

Figure 3. Expression of N-terminal truncated TtpA in HEK 293 cells. (**A**) shows the expression patterns of enhanced GFP alone (GFP), and three different GFP fusions with: the N-terminal truncated version of WT TtpA (WT), a zinc finger mutant of the same truncated TtpA (C246T), and a C-terminal mutation of the same truncated version of TtpA (mut CNBD). Note the nuclear and cytoplasmic expression of GFP alone (GFP), and the predominantly cytoplasmic expression of TtpA and its two mutants. The white bar in each panel indicates the magnification scale (200 μm). In (**B**), the upper panel is a western blot of HEK 293 cell extracts showing the expression of immunoreactive GFP fusions with GFP alone (lane 1), the N-terminal truncated version of WT TtpA (lane 2), zinc finger (C246T) mutated TtpA (lane 3), and the C-terminal mutated (mut CNBD) TtpA (lane 4). The full-length fusion proteins are the uppermost bands in lanes 2–4. The lower panel in B. shows the same blot probed with an antibody to beta actin. (**C**) is an autoradiogram of a northern blot showing the effect of expression of GFP alone, or the indicated GFP fusions with WT and mutant TtpA, on the expression of a co-transfected target mRNA (Mlp-TNF3′) in HEK 293 cells, either in the presence or absence of actinomycin D (ActD) for 1 h, as indicated. 'endo' refers to endogenous mRNA, used as an internal control. (**D**) shows PhosphorImager quantitation of three identical experiments to that shown in C., in which all values were normalized to the average value of GFP alone without ActD. Shown are the mean values ±SD of these three experiments. *$P = 0.002$ when comparing the average WT value to the average GFP value after 1 h of ActD, using a one-tailed Student's *t* test with Bonferroni correction; the same comparisons of the two mutant proteins to GFP after 1 h of ActD were not significant. No statistical tests were applied to the steady state values because the GF*P* values were normalized to 1.

but were not seen in the revertant of the same mutant *ttpA*$^{E236fsx\text{-}rev}$ (Supplemental Figure S1). However, when the null cells were grown on plastic surfaces ('surface culture'), the nuclear staining and slow growth phenotypes were not observed in the null mutants (Supplemental Figure S1). Therefore, unless otherwise specified, the RNA-Seq and NanoString data described below were from cells grown to approximately 80% confluence on plastic dishes under axenic conditions.

We performed five independent RNA-Seq experiments on polyA+-selected RNA from cultures containing the null mutations *ttpA*^{C240ins}, *ttpA*^{E236fsx}and *ttpA*^{Y242fsx}, as well as on the TZF domain point mutant, *ttpA*^{C231S} (Figure 1A), and compared these to WT cells grown and processed in parallel. For the initial RNA-Seq analyses, our initial cutoffs for inclusion were: minimum average normalized reads per kb in the WT cells of 21, equivalent to approximately 1 FPKM; raw fold ratios of 2 or more when comparing averages of the data from null mutant cells with those from WT cells; and adjusted *P* values of < 0.05. We later expanded the fold-change criterion to include transcripts whose raw fold ratios were 1.4 or greater, leaving the other criteria the same.

When data from all five experiments were compared (see Figure 4 and Supplemental Figure S2), only three upregulated and no downregulated transcripts met all the criteria in all datasets, including the raw fold ratio of greater than 2. These three transcripts were highly abundant. For example, in WT cells in surface culture, *DD3-3* mRNA was the 92nd most abundant transcript, *sodC* was the 104th, and *DDB_G0281067* was the 117th, of the more than 12,000 transcripts detected. For comparison, average *TtpA* mRNA levels in the same WT samples ranked 1176th in abundance. In one of the null mutants under the same conditions, levels of the target transcripts increased markedly, so that *DD3-3* mRNA was the third most abundant transcript, *sodC* was the 12th, and *DDB_G0281067* was the 67th. As in this example, all three were upregulated in the mutant strains by more than several-fold, with adjusted *P* values of less than the software's reportable minimum of 1e–325 in most cases. These three transcripts will be referred to here as the 'top tier' targets of TtpA. These RNA-Seq data are shown in the four panels of Figure 4, each panel labeled with one of the three top tier TtpA target transcripts, *sodC*, *DD3-3* and *DDB_G0281067* mRNAs, as well as an unrelated housekeeping gene, *snpA*, as one of many control examples. Each panel shows the effects of genetic manipulations and culture changes on the mRNA levels of that one transcript. Within each panel, group A shows the effect of three of the proposed null mutants on the accumulation of the target transcripts in cells grown in surface culture. In each case, there was a large fold increase in all three transcripts in all three mutants, whereas the expression of *snpA* mRNA was largely unchanged. The groups labeled B in each panel showed the effect of the C-terminal truncation, *ttpA*^{D450trx}, on accumulation of the same three transcripts; remarkably, these expression levels were also upregulated similarly to those of the transcripts in the three null mutants.

In the groups labeled C, the behavior of the three potential top tier target transcripts was compared between

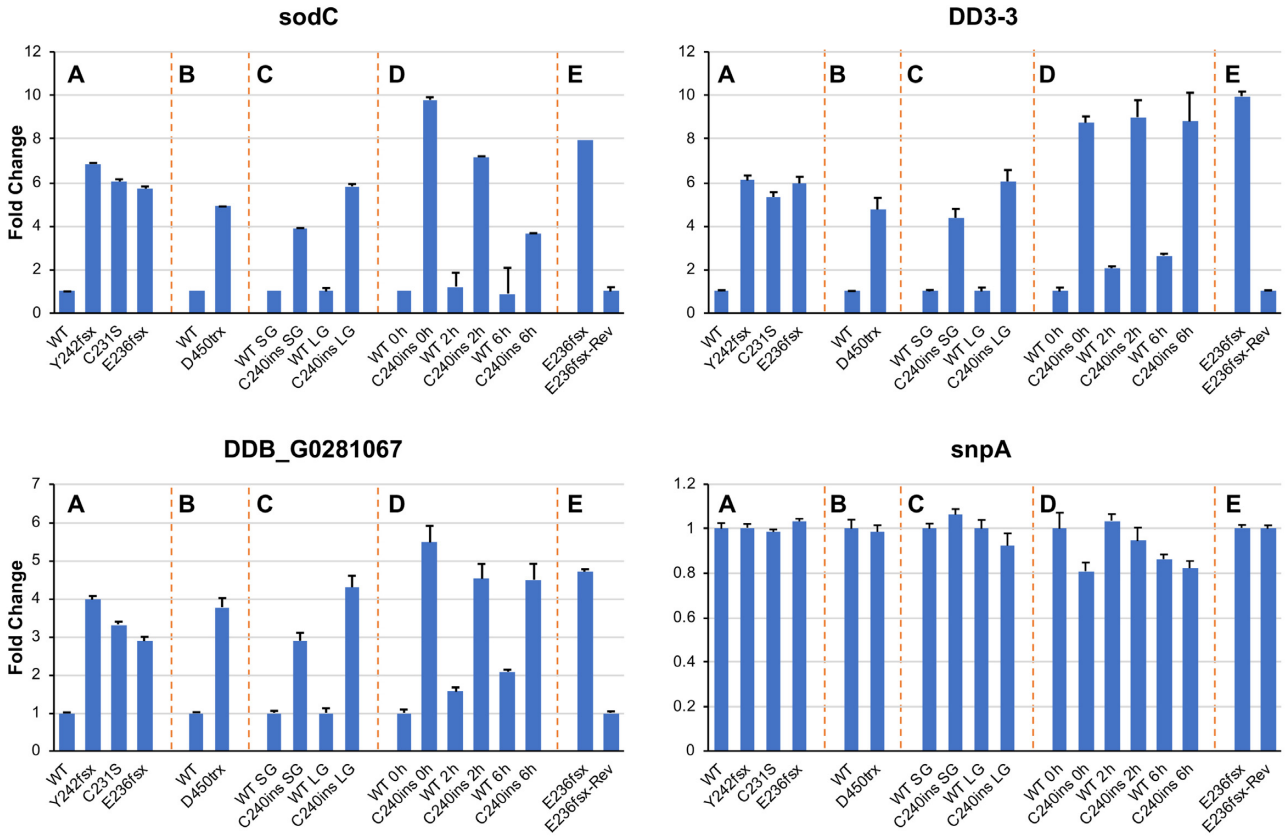

Figure 4. RNA-Seq data showing expression of the three top tier target transcripts in the various loss of function mutants. Each of the four panels shows RNA-Seq results for an individual mRNA, including the three top tier TtpA target transcripts (*sodC*, *DD3-3* and *DDB_G0281067* mRNAs, as labeled), and a housekeeping control, *snpA*. Groups A in each panel show mRNA expression data from surface cultures of vegetative amebae from three different null mutants, as indicated, with average mutant expression values shown as fold changes over the average WT value for that experiment, +/- SD. Groups B show the effect of the C-terminal truncation mutant, normalized to the WT average, in the same experiment. Groups C show similar expression data for another of the null mutants in both surface and liquid culture; in each case, normalization was to the respective WT mean. Groups D show the effect of several hours of nutrient starvation-induced differentiation in surface culture, using the time 0 WT average as the normalizing factor for the entire experiment. Groups E show the effect of the reversion mutant on the expression of the frame shift mutant $ttpA^{E236fsx}$—in this case, the average of the reversion values is set at 1, and the mutant values are normalized to that average. The data from groups E were generated using NanoString nCounter technology; all the other data are from RNA-Seq experiments. In groups A–D, adjusted *P* values from the DESeq2 analysis, comparing mutant and WT averages from the original data, were usually less than the software's reportable minimum of 1e-325 for all transcripts except for *snpA*. In the E groups, the *P* value from a Bonferroni-corrected Student's two-tailed unpaired t test was < 1e-08 in each case, except in the case of *snpA*, when it was not significant.

surface growth and liquid growth in the WT and null mutant $ttpA^{C240ins}$ cells; there was very little difference in their behavior in the two growth conditions. If anything, the expression differences were even greater between the mutant and WT cells in liquid culture.

We also compared expression during the first six hours of development, initiated upon nutrient removal (45) (groups D within Figure 4). In the WT cells, levels of *ttpA* mRNA increased by 40% at 2 h (from 6707 ± 789 normalized reads per kb (± SD; $n = 3$) to 9419 ± 449) and by 75% (11,773 ± 1515) after 6 h of early development. The three top tier TtpA target mRNAs showed highly (>>2×) elevated levels of expression in the *ttpA* mutant compared to WT, at all developmental time points (groups D within Figure 4).

To assess possible off-target effects, we mutated one of the original TZF domain frameshift mutants, $ttpA^{E236fsx}$, to revert the sequence to WT ($ttpA^{E236fsx\text{-}rev}$), and measured expression levels using NanoString nCounter analyses (see below). The reversion mutant (Figure 4, groups E), had expression levels of all three potential target transcripts that were indistinguishable from WT levels, suggesting that the gene expression phenotypes were solely due to *ttpA* disruption.

To confirm and more precisely quantitate expression changes in the mutants, we measured target transcript levels by NanoString in a new set of experiments. This technique measures transcript levels without amplification (38,39), and normalizes them to spiked-in controls as well as the geometric means of 14 housekeeping transcripts chosen as described in Methods and Materials. The three presumed null mutants tested exhibited consistent, steady-state increases in levels of the three top tier TtpA target transcripts; on average, *DD3-3* mRNA was increased 9.6-fold, *DDB_G0281067* mRNA by 4.4-fold, and *sodC* mRNA by 7.7-fold (Figure 5). For all three transcripts, levels were in the WT range in the reversion mutant (Figure 5). The C-terminal mutant was also associated with large increases in the levels of all three top tier target mRNAs compared to WT (Figure 5), with the increases being similar to those seen

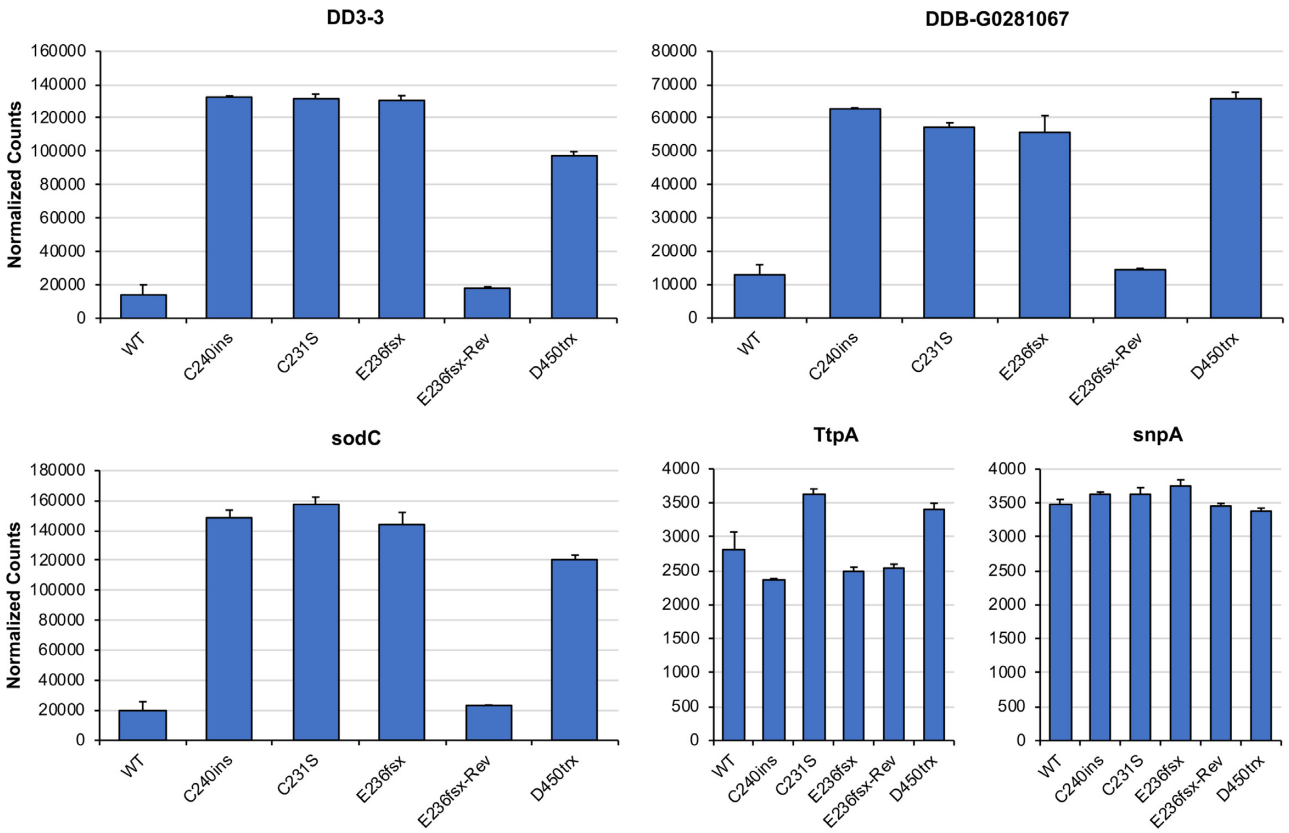

Figure 5. NanoString data on expression of the three top tier target transcripts in the various loss of function mutants. In a separate series of experiments from those shown in Figure 4, amebae in surface culture were analyzed for the expression levels of the same top tier target transcripts in cells expressing some of the same mutants in TtpA shown in Figure 4. In this case, four separate cultures from each strain were used for each mean, ±SD, and all RNA samples were analyzed by NanoString as described in Materials and Methods. In this case, levels of *TtpA* mRNA were also analyzed, using a probe that was based on a sequence 5′ of the encoded TZF domain. See the text for further details.

in the various null mutants. The housekeeping control transcripts, as exemplified by *snpA* (Figure 5), exhibited little difference in expression among all strains.

Interestingly, *ttpA* mRNA levels increased modestly but significantly compared to WT in both the TZF point mutant and C-terminal deletion mutants (increases of 29% and 21%; $P = 0.002$ and 0.012, respectively, based on Bonferroni-corrected, unpaired two-tailed t tests), using a NanoString assay that employed probes directed at sequences 5′ of the TZF domain region (Figure 5). The two null mutants, $ttpA^{C240ins}$ and $ttpA^{E236fsx}$, both expressing abnormal open reading frames for *ttpA* mRNA, may not be directly comparable. The predicted *ttpA* mRNA 3′-UTR is ∼250 nt long, and contains two potential TtpA binding sequences (see below). Thus, TtpA may have a slight but measurable effect on the stability of its own mRNA, as observed in the mouse, where TTP slightly but significantly promotes decay of its own mRNA (5).

In terms of its overall abundance, we estimated that *ttpA* mRNA would be present in ∼70 copies per cell, in WT cells in surface culture in normal medium. This corresponds to approximately 319 FPKM, and represents the 1176th most abundant mRNA in these conditions from the more than 12,000 transcripts evaluated.

Northern blots of total cellular RNA showed the expected increase in mRNA levels for the top tier targets in the null cells compared to WT, but there was no evidence of smaller-sized mRNAs resulting from a shortened poly(A) tail length in the WT cells (Figure 6A), as seen with certain mammalian transcripts (5,46). It should be noted that poly(A) tails in *D. discoideum* tend to be much shorter (∼100 nt) than in mammalian cells (16), making potential size differences based on poly(A) tail length less easy to resolve. We attempted to increase size-difference resolution by cutting the full-length transcripts into shorter 3′ fragments, using RNAse H and sequence-specific oligonucleotides, and hybridizing them with specific 3′-probes. Unfortunately, even this considerable shortening of the *DD3-3*, *sodC* and *DDB_G0281067* transcripts did not allow us to detect metastable, deadenylated intermediates in the WT cells (data not shown). We should note that if these deadenylated transcripts were highly unstable, as expected, they would represent only a very minor component of the total mRNA population, and thus might not be detectable with such experimental designs.

Two different DD3-3-specific antisera detected increased expression of DD3-3 protein in total cellular homogenates from the null cells (Figure 6B). Attempts at raising peptide

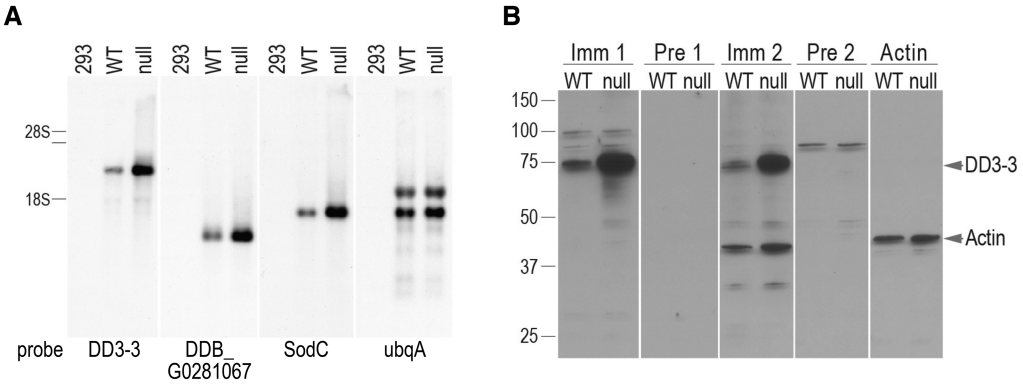

Figure 6. Northern blotting of the three top tier target transcripts, and western blotting of DD3-3, in WT and null cells. In (**A**) are shown three northern blots of the three to tier TtpA target transcripts described in Figures 4 and 5, demonstrating increases in mRNA levels in each case in the mutant compared to the WT cells. Equal amounts of total cellular RNA from human HEK 293 cells were run in the first lane of each blot. Locations of the ribosomal RNAs are indicated to the left of the blots. *ubqA* mRNA was used as an internal normalization control. 28S indicates the migration position of a HEK 293 cell ribosomal RNA, the unlabeled bar indicates the position of the *D. discoideum* 27S ribosomal RNA, and 18S denotes the migration positions of a smaller ribosomal RNA in both HEK 293 cells and *D. discoideum*. In (**B**) is shown a western blot of DD3-3 in WT and *ttpA* null mutant cells, showing immunoreactivity with two different anti-peptide antisera (Imm 1 and Imm 2), along with their respective pre-immune sera (Pre 1 and Pre 2). A parallel blot probed for actin is shown on the right. The positions of M_r standards in thousands are shown to the left of the blots, and the positions of DD3-3 and actin are indicated to the right of the blots.

antisera against the other two top tier targets were not successful.

We also broadened our selection criteria to include transcripts whose raw fold-change ratios were reduced, so that mRNAs were identified that had only 1.4-fold increases in the loss of function mutants in all datasets. We identified three other transcripts whose levels were persistently and significantly up-regulated within these criteria (see volcano plots in Supplemental Figure S2, and RNA-Seq data in Supplemental Figure S3). No down-regulated transcripts met these new criteria. The three new transcripts, which we will refer to as 'second tier' targets, were *noxA*, *cybA* and *DDB_G0278313* mRNAs. All exhibited elevated expression in the multiple mutants compared to WT, but these fold-change increases were generally much lower than those of the top tier transcripts *DD3-3*, *sodC* and *DDB_G0281067* (see Supplementary Figure S2).

Potential TTP family member binding sites in all TtpA target transcripts

We identified likely full-length 3′-UTRs for the *DD3-3*, *sodC* and *DDB_G0281067* transcripts, and examined them for possible TTP family member binding sites, exemplified by the optimum single binding site UUAUUUAUU in other organisms. Although this is generally thought to represent an optimum single binding sequence, nucleotide changes in the 1 and 9 position can be tolerated (29), and oligonucleotides with varying numbers of internal U residues can still bind to TZF domain peptides with reasonably high affinity (47). The AU-rich, TTP-binding region is often expanded to include clustered, overlapping internal multimeric motifs, as UU(AUUU)*n*AUU. Genomic sequences including these proposed 3′-UTRs are shown in Figure 7A, with the stop codons shown in bold type; the proposed TTP family member binding site domains in red; the putative polyadenylation signals (AATAAA) in underlined bold type; and the approximate site of polyadenylation indicated by a caret. Although the 3′-UTRs are relatively short in each case, each transcript contained a series of consecutive potential binding sites, capable of binding at least two TTP family proteins. Interestingly, the clustered TTP-binding sites in two of the transcripts occurred 3′ of the polyadenylation signals, a pattern that is not generally found in targets in animals.

We also performed a similar analysis of the 3′UTRs for the three second tier transcripts, and each of them also contained potential clustered, multimeric TTP family member binding sites (Supplemental Figure S3D).

To test whether one of these sequences would confer TtpA susceptibility to a heterologous transcript, we constructed expression vectors consisting of an actin promoter, a GFP coding sequence, and ∼950 nt of genomic sequence containing the proposed 3′-UTR of *sodC* mRNA, which we estimate to be ∼117 nt (Figure 7A, B). This construct was transfected into WT and $ttpA^{C240ins}$ cells, and levels of GFP and the three TtpA target mRNAs were analyzed by NanoString. Levels of the three proposed TtpA target transcripts were increased in the mutant cells; likewise, the *GFP-sodC* fusion mRNA levels were also increased in the mutant cells (Figure 7C). To confirm the effect of the putative TtpA binding sites on transcript levels, and on levels of the expressed protein, we compared GFP expression from the vector containing the WT 3′UTR of *sodC* mRNA to one with mutations in several key adenosine residues in the proposed TtpA binding sites (Figure 7D), under regulation by the same promoter. As expected, GFP fused with the WT 3′-UTR of *sodC* mRNA (Figure 7D) was expressed to greater levels in $ttpA^{C240ins}$ nulls than in the WT cells (Figure 7E). Even greater amounts of GFP were expressed in WT cells when GFP was fused to the mutant *sodC* 3′-UTR sequence. GFP expression did not increase further when GFP fused to the mutant *sodC* sequence was expressed in the mutant $ttpA^{C240ins}$ cells (Figure 7E). These experiments confirmed that the proposed TtpA binding sites in the *sodC* mRNA represent an instability motif, and that there was

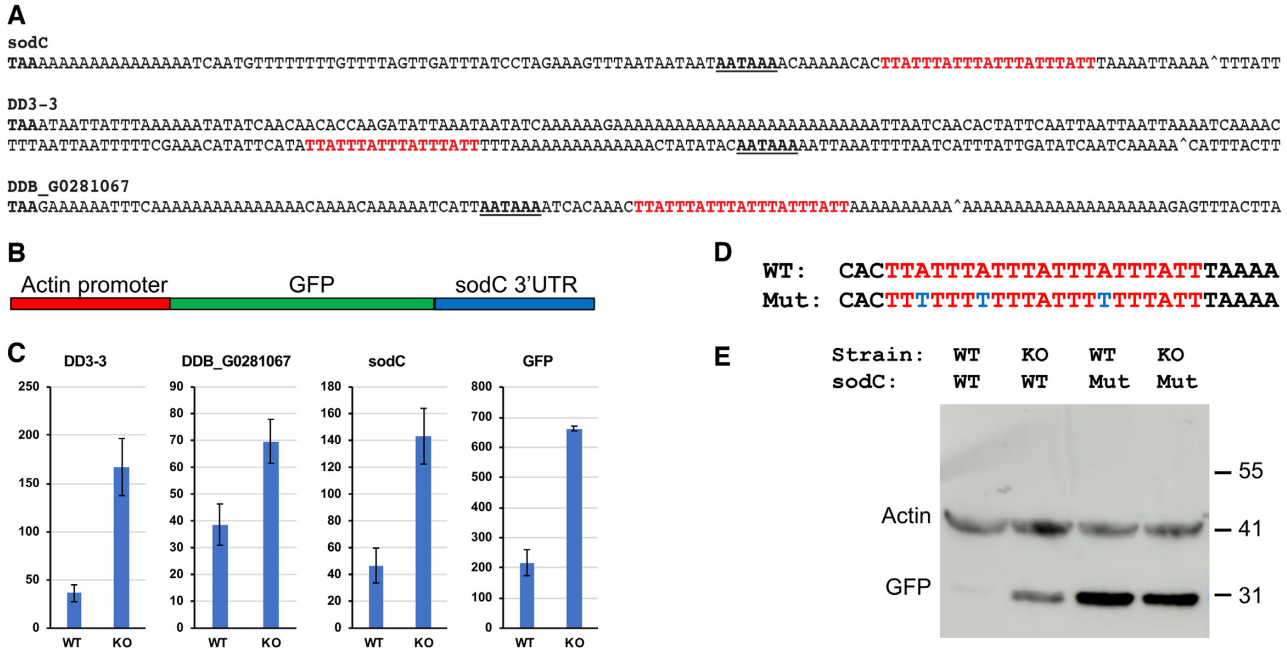

Figure 7. 3′-UTR sequences from the three tier TtpA target transcripts, and effect on expression. Shown in (**A**) are *D. discoideum* genomic sequences 3′ of the stop codon (TAA in bold type) for each of the three top tier TtpA target transcripts discussed in this study. Potential polyadenylation signals are in bold type and underlined, and the approximate positions for post-transcriptional polyadenylation of the transcripts are indicated by a caret symbol. These were based on the UCSC browser tracks from the RNA-Seq data in this study, and were supported in most cases by ESTs or SRA reads. Potential TTP family member core binding sequences (TATTTAT) are indicated in red type. (**B**) shows a schematic representation of an expression construct containing a *D. discoideum* actin promoter, GFP protein coding sequences, and 3′ genomic sequence from *sodC* containing ∼117 nt coding the 3′-UTR and ∼830 b of downstream genomic sequence. (**C**) shows NanoString quantitation (means ± SD of duplicate experiments) of the three top tier TtpA target transcripts as well as of GFP mRNA in WT and null mutant *ttpA*^{C240ins} (null) cells. (**D**) shows the sequences for the WT and mutant (Mut) TtpA binding sites contained in the WT and mutant expression plasmids, and E. shows GFP protein expression in either WT and null mutant (KO) cells expressing either the WT or mutant GFP plasmids described in (D). Actin immunoreactivity is shown as a loading control. See the text for further details.

increased expression of both the WT mRNA and GFP protein in the mutant *ttpA*^{C240ins} cells, consistent with increased GFP mRNA stability in those cells.

We also examined the occurrence of potential TTP binding sites in our three top tier target mRNAs in other dictyostelids by first searching for the encoded proteins in GenBank, and then identifying proximal 3′-UTRs within 243 nt of the stop codons. All three target transcripts fit the same general pattern. Probable orthologues for each of the three TtpA target mRNAs were identified in all of the genomes of group 4 dictyostelid species shown in Figure 8, using a well-established distance tree for dictyostelids (41), and all contained multiple, often consecutive UAUUUAU potential binding sites in their 3′-UTRs. While likely orthologues for each of the TtpA target transcripts were identified in the genomes of the group 3 species, apart from *D. polycephalum* none of their mRNAs contained UU(AUUU)nAUU multimeric binding sites in their 3′-UTRs. While probable orthologues for each of the TtpA targets were identified in the genomes of groups 1 and 2 species, none of their mRNAs possessed tandem or multiple UAUUUAU binding sites in their 3′-UTRs.

The absence of TTP target sequences in evolutionarily distanced mRNA is similar to that seen in other organisms (13,17,18), in which the proteins encoded by the target transcripts may be conserved among distantly related species, but potential TTP binding sites within their 3′-UTRs, and hence possible regulation by TTP family proteins, are not.

Membrane topology and differentiation expression similarities among the putative TtpA targets

The three top tier TtpA target transcripts encode proteins with different predicted biochemical functions. DD3-3 was initially identified in differential display experiments designed to identify transcripts differing in expression between WT cells and cells defective in *O*-glycosylation (48). Cells deficient in DD3-3 developed and aggregated somewhat earlier than WT cells, consistent with the exhibited downregulation of Reg A, an intracellular cAMP-phosphodiesterase, during early development. DD3-3 has an apparent orthologue in many metazoa, including the ascidian *Halocynthia roretzi*, or 'sea pineapple', in which it appears to serve as a self-marker protein that can play a role in contact regulation (49).

SodC was originally identified as one of three extracellular Cu/Zn superoxide dismutases in *D. discoideum* (50). Cells deficient in SodC developed a multi-nuclear phenotype in shaking cell culture. SodC is glycosylphosphatidylinositol (GPI)-anchored, and its knockout led to increases in RasG activity, and defects in chemoattractant sensing, cell polarization and motility (51). These authors suggested that 'SodC and RasG proteins are essential part of a novel inhibitory mechanism that discourages oxidatively stressed cells from chemotaxis', and thus suppresses their development (52).

Less is known about DDB_G0281067, which is listed in dictyBase as a 'putative transmembrane protein'. It is

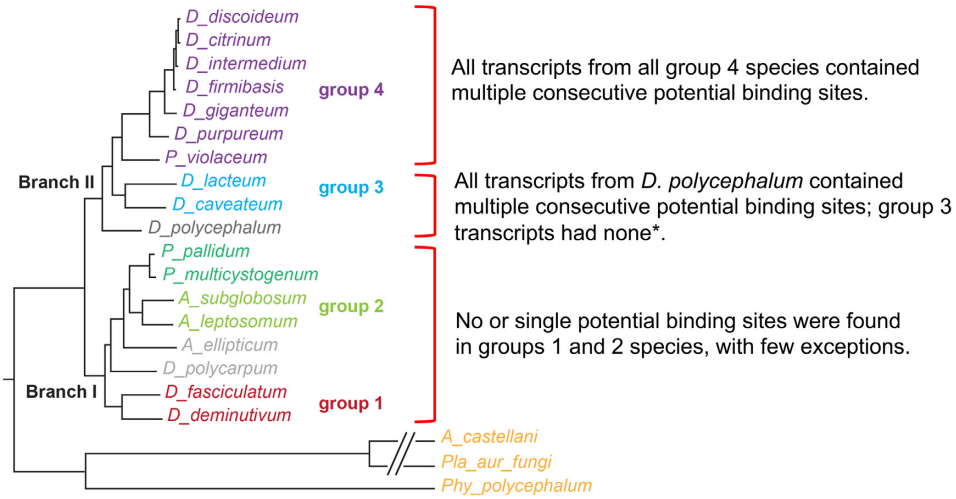

Figure 8. Phylogenetic distribution of the 3′-UTR sequences from the three top tier TtpA target transcripts. Shown is a redrawn phylogenetic tree of dictyostelids that includes the species shown in Figure 1A in (41); full species names are listed in that paper. Unless otherwise noted, we found orthologues for the three proteins encoded by the probable top tier TtpA targets, and then identified likely 3′-UTRs from their respective genomic sequences, using 243 nt 3′ from and including the stop codons. In general, all species in group 4 contained multiple contiguous potential TtpA binding sites in all three target transcripts, and species from the other groups did not. Exceptions are noted in the figure. Two of the three target proteins were not found in *Speleostelium caveatum*. However, DD3-3 was found in that species, and contained a single distal potential binding site.

encoded on chromosome 3, whereas the two others are encoded on chromosome 4.

Of the second tier targets identified that were less highly upregulated in the *ttpA* loss of function mutants, *noxA* mRNA encodes a superoxide-generating NADPH oxidase flavocytochrome A that is involved in generating superoxides for cell defense (53). CybA is a light subunit of another superoxide-generating NADPH oxidase (53). DDB_G0278313 is predicted to encode a pectin lyase-like family protein (20,21).

We next evaluated the predicted membrane topology of all six proteins, using Phobius (http://phobius.sbc.su.se/). All three proteins encoded by the three top tier target transcripts exhibited the same predicted membrane topology (Figure 9A–C), with N-terminal signal peptides, large predicted extracellular segments, single C-terminal transmembrane domains, and short C-terminal cytoplasmic tails. The three second tier target transcripts also encoded predicted membrane proteins, but with different structural organization motifs than those of SodC, DD3-3 and DDB_G0281067 (see Figure 9). The fact that all six target transcripts encode membrane proteins suggested the possibility of a TtpA-dependent post-transcriptional 'RNA regulon', as proposed by Keene and colleagues (26–28). Although absolute levels of the various transcripts will ultimately be influenced by individual promoter strength and regulation, all six transcripts may be subject to similar suppression by TtpA-regulation, and exhibit similar expression patterns during growth and early development (see Figure 4 and Supplemental Figure S3). The data suggest common regulatory dependence during these life cycle stages. The three top tier TtpA target transcripts are highly expressed during growth and very early development (Figures 4 and 9), but are very poorly expressed in stalks, cup cells and spore cells in mature fruiting bodies (54). In contrast, the pattern of TtpA mRNA expression was completely different, with the highest expression observed in the stalks of the mature fruiting body (Figure 9D).

DISCUSSION

Evaluation of the RNA-binding TZF domain from *D. discoideum* TtpA showed that it meets the criteria for inclusion into the greater TTP family of proteins (3). Expression in mammalian cells suggested that the TtpA protein could promote the decay of transcripts containing typical AU-rich binding motifs in their 3′UTRs, and that this effect was abrogated by a point mutant in one of the zinc-coordinating cysteines in the TZF domain. These experiments also suggested the presence of a nuclear export sequence in TtpA, which functions to promote the cytosolic localization of related proteins in other organisms (44,55,56). The TtpA protein also appeared to contain a typical C-terminal CNOT1 binding (CNB) domain, but mutation of this domain in the mammalian cell transfection experiments resulted in complete loss of function, in marked contrast to previous findings with analogous mutants of *Drosophila* TIS11 and mammalian TTP, which both of which retained considerable activity in cell transfection studies (8,13).

To examine the function of TtpA in the intact organism, we engineered three different null mutants in endogenous *ttpA* using CRISPR-Cas technology, as well as a predicted null mutant in the form of a cysteine to serine mutation of one of the critical TZF domain zinc-coordinating residues. All of these mutations led to an interesting cellular phenotype, in which cells grown with shaking in liquid culture exhibited slow growth and multiple DAPI-staining nuclear foci, whereas the same mutant cells grown on plastic surfaces did not exhibit this phenotype. Similar multinuclear, slow growth phenotypes were initially observed with either knockout of or antisense RNA to myosin heavy chain (57,58), and were described as 'cytokinesis defects'.

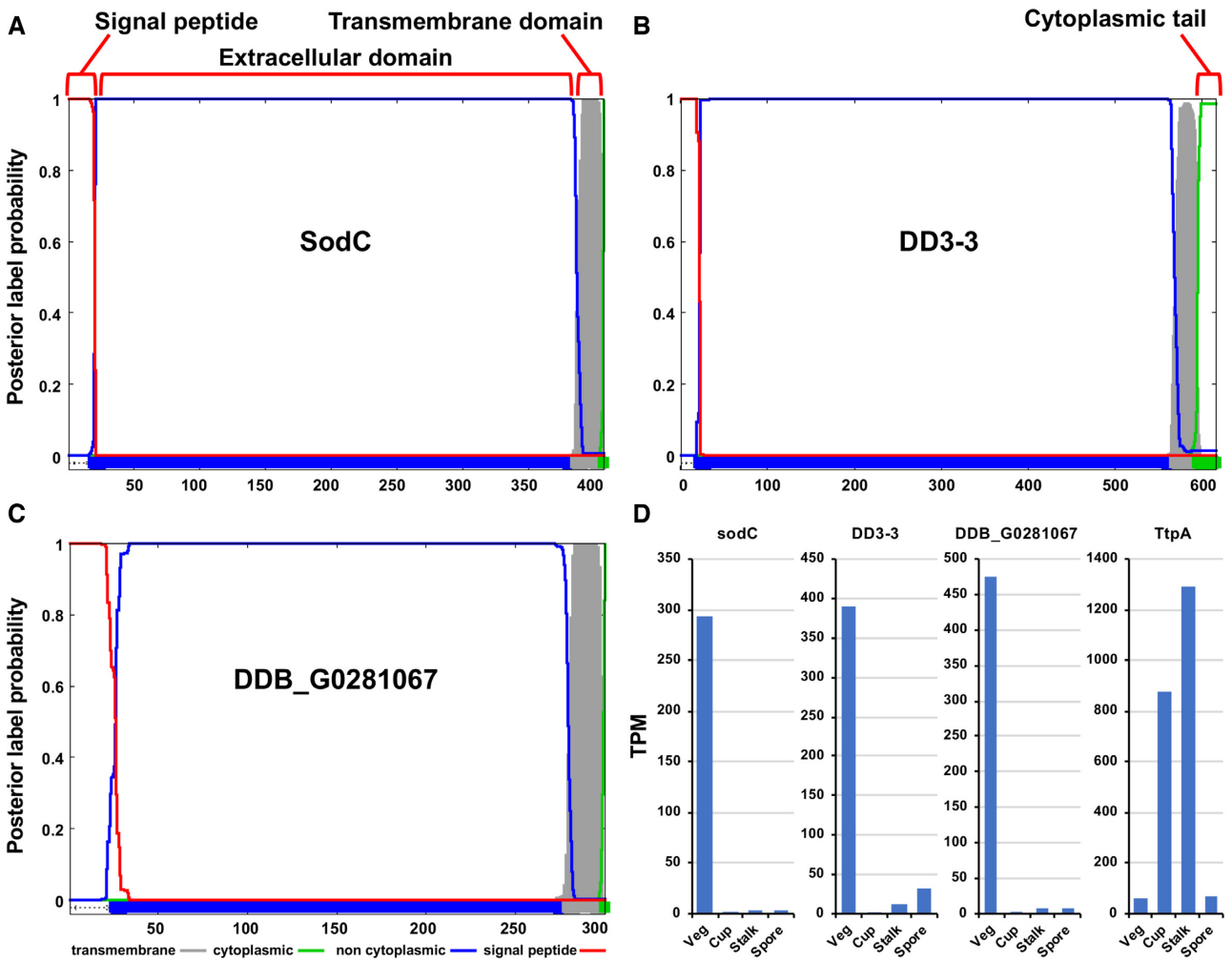

Figure 9. Membrane topology of proteins encoded by the three top tier TtpA target mRNAs, and expression of the transcripts during differentiation into fruiting bodies. For (**A**–**C**), Phobius (http://phobius.sbc.su.se/) was used to calculate membrane topology for the proteins encoded by each of the TtpA target transcripts, as indicated. In the lower right panel (**D**), RNA-Seq data are shown from the dataset deposited by Schaap and colleagues (54), and show the expression of the three top tier TtpA target transcripts, and TtpA mRNA itself, in growing cells and after purification of specific structures from the fully differentiated fruiting bodies. Data are expressed in TPM (transcripts per million), and can be used to compare the expression levels of the TtpA targets, and TtpA mRNA itself, in the different cells and structures. $N = 3$ in each group except 'veg' (vegetative amebae), in which $n = 2$.

This phenotype was later shown to occur when the cells were grown in liquid medium with shaking, and largely disappeared when cultured on plastic surfaces (59). Since then, many other mutants have been shown to exhibit similar phenotypes (reviewed in (60)). These have been divided into type I and II cytokinesis defects, with type I exhibiting multinucleation during surface growth, and type II exhibiting multinucleation and loss of cell division only in liquid culture (60). This unusual phenotype has formed the basis for the genome wide screens that have identified several new genes involved in cytokinesis (61–63), although to our knowledge *ttpA* has not been identified by this means. It is possible that the overexpression of one or more of the proteins encoded by TtpA target transcripts leads to this interesting phenotype, but this remains to be determined.

We therefore performed most of our RNA-Seq analyses on cells growing in axenic surface culture. From the combined RNA-Seq studies, only three 'top tier' transcripts accumulated significantly by more than two-fold in all of the mutants, and three additional 'second tier' transcripts were up-regulated with a more minimal 1.4-fold increase in all of the mutants. These changes were supported by separate experiments using NanoString and northern blotting, and, in the case of *DD3-3* mRNA, were reflected in increased protein expression. The three top tier TtpA target transcripts were all very abundant, and all exhibited large fold changes in the null mutants; they also contained multiple, contiguous copies of the proposed optimal TtpA binding site UUAUUUAUU within their rather short 3′-UTRs. One of the null mutants was converted to a WT sequence by further rounds of CRISPR-Cas mutagenesis, and, reassuringly, the expression levels of the three top tier TtpA target transcripts reverted to normal, as did the DAPI staining pattern in liquid culture (Supplmental Figure S1). *D. discoideum* has a 34 Mb haploid genome, with > 12,000 protein coding genes, and an overall GC content of only 22.4% (64). This extreme AT-richness, combined with the generally short 3′UTRs and relatively poor delineation of these UTRs in

the databases, make it difficult to estimate the number of potential TTP family protein binding sites transcriptome-wide. However, when we searched 100 nt downstream of the stop codons from all 12,940 available transcripts, 2988 transcripts contained one or more UAUUUAU core binding sequences (23.1%), whereas 1098 transcripts (8.5%) contained two or more potential binding sites. These numbers increased with increasing 3′-UTR length, but would decrease significantly if searches demanded at least three sequence motif repeats, as observed with all six of the defined target transcripts. Although a UUAUUUAUU motif or one of its variants is essential for TTP binding and regulation, its presence is not sufficient for TtpA regulation, and additional structural context within the entire 3′-UTR is likely to be highly influential (29).

We also showed that a transcript containing GFP coding sequences fused to a *sodC* 3′-UTR was stabilized in a *ttpA*-null mutant, compared to its expression in WT cells; likewise, mutation of the UUAUUUAUUUAUUUAUUUAUU element to UU**U**UUU**U**UUUA**U**UU**U**UUUA**U**U in the *sodC* 3′-UTR markedly increased GFP mRNA expression levels in WT cells. These results do not definitively establish this and the other transcripts as direct TtpA destabilizing targets, although the evidence to date is powerful. Other types of data to support this conclusion could include: Direct evidence of different polyA tail lengths in mutants compared to WT cells, as has been found in some systems (5,46); co-immunoprecipitation of target mRNA with TtpA; demonstration of deadenylation- and decay-promoting activities in cell-free experiments; and direct demonstration of decreased decay rates of the endogenous transcripts in null mutants.

Based on previous studies in other organisms and in vitro, we predicted that mutation of any one of the TZF domain cysteines and histidines would result in complete loss of function (see (5) and references therein). This appeared to be the case, in that all six proposed TtpA target transcripts accumulated to the same extent in the TZF domain point mutant as in the three null mutants, and the point mutant also exhibited the multinuclear, slow-growth phenotype in liquid culture. Similarly, we expected that deletion of the C-terminal CNB domain would lead to only a modest loss of activity, as seen in previous cell transfection studies (8,13) and in knock-in mice (14). However, in sharp contrast, the C-terminal truncation in *D. discoideum* led to increases in target transcript expression in all six cases that were very similar to those seen in the null mutants, as well as a typical cytokinesis defect phenotype in liquid culture. These findings suggest the intriguing possibility that, in *D. discoideum*, most or all TtpA activity is dependent on the presence of the C-terminal CNB domain. This difference from mammals raises the possibility that there may be evolutionary differences in how TTP family proteins interact with the cellular deadenylation machinery.

Another important finding was that six closely related (group 4) dictyostelid species expressed transcripts that contained multiple, contiguous, likely 3′-UTR binding sites in orthologues of all three top tier targets, but orthologous transcripts from species that were more distantly related either lacked or had fewer binding sites. This is similar to what was found previously in other organisms (13,17,18), and suggests that the more distantly related dictyostelids might have evolved target transcripts that differ from the ones described here. It will be interesting to test this possibility in one or more of these distantly related species.

Although the three proteins described here as encoded by the top tier TtpA target transcripts may have different biochemical activities, they exhibited striking and essentially identical membrane topologies, with N-terminal signal sequences, long extracellular domains, single transmembrane domains near the C-terminus, and very short cytoplasmic tails. In the case of sodC, the protein is known to be a glycosylphosphatidylinositol-anchored plasma membrane protein (51), but nothing is known about the glycosylation patterns or membrane localizations of the of the others. The three second tier target transcripts also encoded predicted membrane proteins. In addition to the membrane localization of the proteins, the up-regulated transcripts were co-regulated in several different life cycle stages, with high-level expression in growing cells and early development. Five of the genes showed drastically decreased expression during late development (54). There were major increases in *ttpA* mRNA expression in the cup cells and stalks of fruiting bodies during late development and it will be of great interest to determine whether new TtpA target transcripts will emerge in comparisons of differentiated tissues from WT and *ttpA* KO strains.

The membrane localization of the proteins encoded by the target transcripts, and their mostly parallel behavior during differentiation, suggest the possibility that these transcripts are behaving as a post-transcriptional 'RNA regulon', defined by Keene as '… a model in which mRNAs that encode functionally related proteins are coordinately regulated during cell growth and differentiation as post-transcriptional RNA operons or regulons, through a ribonucleoprotein-driven mechanism' (65). In this case, we define 'functionally related proteins' to include proteins with membrane localization and similar transcript expression behavior during differentiation. Such a concept might be extended to include a previous study on chemotaxis in *Dictyostelium*, where the mRNA 3′UTR binding protein Puf118 could localize the mRNAs encoding proteins from several different chemotaxis pathways to the chemotactic front (66). The primary activity of TtpA is to promote mRNA deadenylation and decay in a specific mRNA subclass. Nonetheless, future studies will determine whether TtpA has separate effects on target transcript and protein localization.

DATA AVAILABILITY

The sequence of full-length TtpA described in this paper has been deposited in GenBank, accession number MT946549. RNA-Seq datasets described in this paper have been deposited in GEO, accession number GSE156813.

SUPPLEMENTARY DATA

Supplementary Data are available at NAR Online.

ACKNOWLEDGEMENTS

We are grateful to our colleagues at the NIEHS Epigenomics and DNA Sequencing Core Laboratory and the NanoString Technologies, Inc. Proof of Principle Lab for analyses, and to Monica Pillon and Michael Fessler for thoughtful comments on the manuscript.

FUNDING

Intramural Research Programs of the NIEHS and NIDDK, both components of the National Institutes of Health. Funding for open access charge: Intramural research funds from the NIEHS and NIDDK.

Conflict of interest statement. A.R.K. is Executive Editor of *NAR*.

REFERENCES

1. Brooks,S.A. and Blackshear,P.J. (2013) Tristetraprolin (TTP): interactions with mRNA and proteins, and current thoughts on mechanisms of action. *Biochim. Biophys. Acta*, **1829**, 666–679.
2. Wells,M.L., Perera,L. and Blackshear,P.J. (2017) An ancient family of RNA-binding proteins: still important! *Trends Biochem. Sci.*, **42**, 285–296.
3. Lai,W.S., Wells,M.L., Perera,L. and Blackshear,P.J. (2019) The tandem zinc finger RNA binding domain of members of the tristetraprolin protein family. *Wiley Interdiscip. Rev. RNA*, **10**, e1531.
4. Lai,W.S., Kennington,E.A. and Blackshear,P.J. (2002) Interactions of CCCH zinc finger proteins with mRNA: non-binding tristetraprolin mutants exert an inhibitory effect on degradation of AU-rich element-containing mRNAs. *J. Biol. Chem.*, **277**, 9606–9613.
5. Lai,W.S., Stumpo,D.J., Qiu,L., Faccio,R. and Blackshear,P.J. (2018) A knock-in tristetraprolin (TTP) zinc finger point mutation in mice: comparison with complete TTP deficiency. *Mol. Cell. Biol.*, **38**, e00488-17.
6. Wells,M.L., Hicks,S.N., Perera,L. and Blackshear,P.J. (2015) Functional equivalence of an evolutionarily conserved RNA binding module. *J. Biol. Chem.*, **290**, 24413–24423.
7. Blackshear,P.J. and Perera,L. (2014) Phylogenetic distribution and evolution of the linked RNA-binding and NOT1-binding domains in the tristetraprolin family of tandem CCCH zinc finger proteins. *J. Interferon Cytokine Res.*, **34**, 297–306.
8. Fabian,M.R., Frank,F., Rouya,C., Siddiqui,N., Lai,W.S., Karetnikov,A., Blackshear,P.J., Nagar,B. and Sonenberg,N. (2013) Structural basis for the recruitment of the human CCR4–NOT deadenylase complex by tristetraprolin. *Nat. Struct. Mol. Biol.*, **20**, 735–739.
9. Lykke-Andersen,J. and Wagner,E. (2005) Recruitment and activation of mRNA decay enzymes by two ARE-mediated decay activation domains in the proteins TTP and BRF-1. *Genes Dev.*, **19**, 351–361.
10. Sandler,H., Kreth,J., Timmers,H.T. and Stoecklin,G. (2011) Not1 mediates recruitment of the deadenylase Caf1 to mRNAs targeted for degradation by tristetraprolin. *Nucleic. Acids. Res.*, **39**, 4373–4386.
11. Bulbrook,D., Brazier,H., Mahajan,P., Kliszczak,M., Fedorov,O., Marchese,F.P., Aubareda,A., Chalk,R., Picaud,S., Strain-Damerell,C. *et al.* (2018) Tryptophan-mediated interactions between tristetraprolin and the CNOT9 subunit are required for CCR4–NOT deadenylase complex recruitment. *J. Mol. Biol.*, **430**, 722–736.
12. Webster,M.W., Stowell,J.A. and Passmore,L.A. (2019) RNA-binding proteins distinguish between similar sequence motifs to promote targeted deadenylation by Ccr4-Not. *Elife*, **8**, e40670.
13. Choi,Y.J., Lai,W.S., Fedic,R., Stumpo,D.J., Huang,W., Li,L., Perera,L., Brewer,B.Y., Wilson,G.M., Mason,J.M. *et al.* (2014) The Drosophila Tis11 protein and its effects on mRNA expression in flies. *J. Biol. Chem.*, **289**, 35042–35060.
14. Lai,W.S., Stumpo,D.J., Wells,M.L., Gruzdev,A., Hicks,S.N., Nicholson,C.O., Yang,Z., Faccio,R., Webster,M.W., Passmore,L.A. *et al.* (2019) Importance of the conserved carboxyl-Terminal CNOT1 binding domain to tristetraprolin activity in vivo. *Mol. Cell. Biol.*, **39**, e00029-19.
15. Cuthbertson,B.J., Liao,Y., Birnbaumer,L. and Blackshear,P.J. (2008) Characterization of zfs1 as an mRNA-binding and -destabilizing protein in Schizosaccharomyces pombe. *J. Biol. Chem.*, **283**, 2586–2594.
16. Jacobson,A., Firtel,R.A. and Lodish,H. (1974) Transcription of polydeoxythymidylate sequences in the genome of the cellular slime mold, Dictyostelium discoideum. *Proc. Natl. Acad. Sci. U.S.A.*, **71**, 1607–1611.
17. Wells,M.L., Huang,W., Li,L., Gerrish,K.E., Fargo,D.C., Ozsolak,F. and Blackshear,P.J. (2012) Posttranscriptional regulation of cell-cell interaction protein-encoding transcripts by Zfs1p in Schizosaccharomyces pombe. *Mol. Cell. Biol.*, **32**, 4206–4214.
18. Wells,M.L., Washington,O.L., Hicks,S.N., Nobile,C.J., Hartooni,N., Wilson,G.M., Zucconi,B.E., Huang,W., Li,L., Fargo,D.C. *et al.* (2015) Post-transcriptional regulation of transcript abundance by a conserved member of the tristetraprolin family in Candida albicans. *Mol. Microbiol.*, **95**, 1036–1053.
19. Loomis,W.F. (2013) Comparative genomics of the dictyostelids. *Methods Mol. Biol.*, **983**, 39–58.
20. Basu,S., Fey,P., Pandit,Y., Dodson,R., Kibbe,W.A. and Chisholm,R.L. (2013) DictyBase 2013: integrating multiple *Dictyostelid* species. *Nucleic Acids Res.*, **41**, D676–D683.
21. Fey,P., Dodson,R.J., Basu,S. and Chisholm,R.L. (2013) One stop shop for everything *Dictyostelium*: dictyBase and the Dicty Stock Center in 2012. *Methods Mol. Biol.*, **983**, 59–92.
22. Jaiswal,P., Majithia,A.R., Rosel,D., Liao,X.H., Khurana,T. and Kimmel,A.R. (2019) Integrated actions of mTOR complexes 1 and 2 for growth and development of Dictyostelium. *Int. J. Dev. Biol.*, **63**, 521–527.
23. Kimmel,A.R. and Firtel,R.A. (2004) Breaking symmetries: regulation of Dictyostelium development through chemoattractant and morphogen signal-response. *Curr. Opin. Genet. Dev.*, **14**, 540–549.
24. Loomis,W.F. (2014) Cell signaling during development of *Dictyostelium*. *Dev. Biol.*, **391**, 1–16.
25. Nichols,J.M., Veltman,D. and Kay,R.R. (2015) Chemotaxis of a model organism: progress with *Dictyostelium*. *Curr. Opin. Cell Biol.*, **36**, 7–12.
26. Blackinton,J.G. and Keene,J.D. (2014) Post-transcriptional RNA regulons affecting cell cycle and proliferation. *Semin. Cell Dev. Biol.*, **34**, 44–54.
27. Keene,J.D. (2001) Ribonucleoprotein infrastructure regulating the flow of genetic information between the genome and the proteome. *Proc. Natl. Acad. Sci. U.S.A.*, **98**, 7018–7024.
28. Keene,J.D. and Tenenbaum,S.A. (2002) Eukaryotic mRNPs may represent posttranscriptional operons. *Mol. Cell*, **9**, 1161–1167.
29. Hudson,B.P., Martinez-Yamout,M.A., Dyson,H.J. and Wright,P.E. (2004) Recognition of the mRNA AU-rich element by the zinc finger domain of TIS11d. *Nat. Struct. Mol. Biol.*, **11**, 257–264.
30. Emsley,P., Lohkamp,B., Scott,W.G. and Cowtan,K. (2010) Features and development of Coot. *Acta Crystallogr. D. Biol. Crystallogr.*, **66**, 486–501.
31. Lai,W.S., Perera,L., Hicks,S.N. and Blackshear,P.J. (2014) Mutational and structural analysis of the tandem zinc finger domain of tristetraprolin. *J. Biol. Chem.*, **289**, 565–580.
32. Case,D.A., Ben-Shalom,I.Y., Brozell,S.R., Cerutti,D.S., Cheatham,T.E.I., Cruzeiro,V.W.D., Darden,T.A., Duke,R.E., Ghoreishi,D., Gilson,M.K. *et al.* (2018) *Amber 2018*. University of California, San Francisco.
33. Humphrey,W., Dalke,A. and Schulten,K. (1996) VMD: visual molecular dynamics. *J. Mol. Graph.*, **14**, 33–38.
34. Kedar,V.P., Zucconi,B.E., Wilson,G.M. and Blackshear,P.J. (2012) Direct binding of specific AUF1 isoforms to tandem zinc finger domains of tristetraprolin (TTP) family proteins. *J. Biol. Chem.*, **287**, 5459–5471.
35. Lai,W.S., Carballo,E., Thorn,J.M., Kennington,E.A. and Blackshear,P.J. (2000) Interactions of CCCH zinc finger proteins with mRNA. Binding of tristetraprolin-related zinc finger proteins to Au-rich elements and destabilization of mRNA. *J. Biol. Chem.*, **275**, 17827–17837.
36. Blackshear,P.J., Phillips,R.S., Ghosh,S., Ramos,S.B., Richfield,E.K. and Lai,W.S. (2005) Zfp36l3, a rodent X chromosome gene encoding a placenta-specific member of the Tristetraprolin family of CCCH tandem zinc finger proteins. *Biol. Reprod.*, **73**, 297–307.

37. Sekine,R., Kawata,T. and Muramoto,T. (2018) CRISPR/Cas9 mediated targeting of multiple genes in Dictyostelium. *Sci. Rep.*, **8**, 8471.
38. Fortina,P. and Surrey,S. (2008) Digital mRNA profiling. *Nat. Biotechnol.*, **26**, 293–294.
39. Tsang,H.F., Xue,V.W., Koh,S.P., Chiu,Y.M., Ng,L.P. and Wong,S.C. (2017) NanoString, a novel digital color-coded barcode technology: current and future applications in molecular diagnostics. *Expert Rev. Mol. Diagn.*, **17**, 95–103.
40. Pilcher,K.E., Gaudet,P., Fey,P., Kowal,A.S. and Chisholm,R.L. (2007) A general purpose method for extracting RNA from Dictyostelium cells. *Nat. Protoc.*, **2**, 1329–1332.
41. Schilde,C., Lawal,H.M., Kin,K., Shibano-Hayakawa,I., Inouye,K. and Schaap,P. (2019) A well supported multi gene phylogeny of 52 dictyostelia. *Mol. Phylogenet. Evol.*, **134**, 66–73.
42. Gao,C., Liu,C., Schenz,D., Li,X., Zhang,Z., Jusup,M., Wang,Z., Beekman,M. and Nakagaki,T. (2019) Does being multi-headed make you better at solving problems? A survey of Physarum-based models and computations. *Phys Life Rev*, **29**, 1–26.
43. Sun,Q., Carrasco,Y.P., Hu,Y., Guo,X., Mirzaei,H., Macmillan,J. and Chook,Y.M. (2013) Nuclear export inhibition through covalent conjugation and hydrolysis of Leptomycin B by CRM1. *Proc. Natl. Acad. Sci. U.S.A.*, **110**, 1303–1308.
44. Phillips,R.S., Ramos,S.B.V. and Blackshear,P.J. (2002) Members of the tristetraprolin family of tandem CCCH zinc finger proteins exhibit CRM1-dependent nucleocytoplasmic shuttling. *J. Biol. Chem.*, **277**, 11606–11613.
45. Jaiswal,P. and Kimmel,A.R. (2019) mTORC1/AMPK responses define a core gene set for developmental cell fate switching. *BMC Biol.*, **17**, 58.
46. Carballo,E., Lai,W.S. and Blackshear,P.J. (2000) Evidence that tristetraprolin is a physiological regulator of granulocyte-macrophage colony-stimulating factor messenger RNA deadenylation and stability. *Blood*, **95**, 1891–1899.
47. Brewer,B.Y., Malicka,J., Blackshear,P.J. and Wilson,G.M. (2004) RNA sequence elements required for high affinity binding by the zinc finger domain of tristetraprolin: conformational changes coupled to the bipartite nature of Au-rich MRNA-destabilizing motifs. *J. Biol. Chem.*, **279**, 27870–27877.
48. Sakuragi,N., Ogasawara,N., Tanesaka,E. and Yoshida,M. (2005) Functional analysis of a novel gene, DD3-3, from *Dictyostelium discoideum*. *Biochem. Biophys. Res. Commun.*, **331**, 1201–1206.
49. Ema,M., Okada,T., Takahashi,M., Uchiyama,M., Kubo,H., Moriyama,H., Miyakawa,H. and Matsumoto,M. (2019) A self-marker-like protein governs hemocyte allorecognition in Halocynthia roretzi. *Zoological Lett*, **5**, 34.
50. Tsuji,A., Akaza,Y., Nakamura,S., Kodaira,K. and Yasukawa,H. (2003) Multinucleation of the sodC-deficient *Dictyostelium discoideum*. *Biol. Pharm. Bull.*, **26**, 1174–1177.
51. Veeranki,S., Kim,B. and Kim,L. (2008) The GPI-anchored superoxide dismutase SodC is essential for regulating basal Ras activity and for chemotaxis of Dictyostelium discoideum. *J. Cell Sci.*, **121**, 3099–3108.
52. Castillo,B., Kim,S.H., Sharief,M., Sun,T. and Kim,L.W. (2017) SodC modulates ras and PKB signaling in Dictyostelium. *Eur. J. Cell Biol.*, **96**, 1–12.
53. Lardy,B., Bof,M., Aubry,L., Paclet,M.H., Morel,F., Satre,M. and Klein,G. (2005) NADPH oxidase homologs are required for normal cell differentiation and morphogenesis in Dictyostelium discoideum. *Biochim. Biophys. Acta*, **1744**, 199–212.
54. Kin,K., Forbes,G., Cassidy,A. and Schaap,P. (2018) Cell-type specific RNA-Seq reveals novel roles and regulatory programs for terminally differentiated *Dictyostelium* cells. *BMC Genomics*, **19**, 764.
55. Frederick,E.D., Ramos,S.B. and Blackshear,P.J. (2008) A unique C-terminal repeat domain maintains the cytosolic localization of the placenta-specific tristetraprolin family member ZFP36L3. *J. Biol. Chem.*, **283**, 14792–14800.
56. Twyffels,L., Wauquier,C., Soin,R., Decaestecker,C., Gueydan,C. and Kruys,V. (2013) A masked PY-NLS in Drosophila TIS11 and its mammalian homolog tristetraprolin. *PLoS One*, **8**, e71686.
57. De Lozanne,A. and Spudich,J.A. (1987) Disruption of the *Dictyostelium myosin* heavy chain gene by homologous recombination. *Science*, **236**, 1086–1091.
58. Knecht,D.A. and Loomis,W.F. (1987) Antisense RNA inactivation of myosin heavy chain gene expression in *Dictyostelium discoideum*. *Science*, **236**, 1081–1086.
59. Zang,J.H., Cavet,G., Sabry,J.H., Wagner,P., Moores,S.L. and Spudich,J.A. (1997) On the role of myosin-II in cytokinesis: division of *Dictyostelium* cells under adhesive and nonadhesive conditions. *Mol. Biol. Cell*, **8**, 2617–2629.
60. Adachi,H. (2001) Identification of proteins involved in cytokinesis of *Dictyostelium*. *Cell Struct. Funct.*, **26**, 571–575.
61. Adachi,H., Hasebe,T., Yoshinaga,K., Ohta,T. and Sutoh,K. (1994) Isolation of Dictyostelium discoideum cytokinesis mutants by restriction enzyme-mediated integration of the blasticidin S resistance marker. *Biochem. Biophys. Res. Commun.*, **205**, 1808–1814.
62. Larochelle,D.A., Vithalani,K.K. and De Lozanne,A. (1996) A novel member of the rho family of small GTP-binding proteins is specifically required for cytokinesis. *J. Cell Biol.*, **133**, 1321–1329.
63. Vithalani,K.K., Shoffner,J.D. and De Lozanne,A. (1996) Isolation and characterization of a novel cytokinesis-deficient mutant in Dictyostelium discoideum. *J. Cell. Biochem.*, **62**, 290–301.
64. Eichinger,L., Pachebat,J.A., Glockner,G., Rajandream,M.A., Sucgang,R., Berriman,M., Song,J., Olsen,R., Szafranski,K., Xu,Q. *et al.* (2005) The genome of the social amoeba Dictyostelium discoideum. *Nature*, **435**, 43–57.
65. Keene,J.D. (2007) RNA regulons: coordination of post-transcriptional events. *Nat. Rev. Genet.*, **8**, 533–543.
66. Hotz,M. and Nelson,W.J. (2017) Pumilio-dependent localization of mRNAs at the cell front coordinates multiple pathways required for chemotaxis. *Nat. Commun.*, **8**, 1366.
67. Qiu,L.Q., Stumpo,D.J. and Blackshear,P.J. (2012) Myeloid-specific tristetraprolin deficiency in mice results in extreme lipopolysaccharide sensitivity in an otherwise minimal phenotype. *J. Immunol.*, **188**, 5150–5159.